

1 **Novel C-3-(N-alkyl-aryl)-aminomethyl rifamycin SV derivatives exhibit activity against rifampicin-**
2 **resistant *Mycobacterium tuberculosis* RpoB_{S522L} strain and display a different binding mode at the**
3 **RNAP β -subunit site compared to rifampicin**

4 Mire Zloh,^{a,b} Megha Gupta,^c Tanya Parish^d and Federico Brucoli^{e*}

5 ^aFaculty of Pharmacy, University Business Academy, Novi Sad, 2100, Serbia

6 ^bUCL School of Pharmacy, UCL, London WC1N 1AX, UK

7 ^cInfectious Disease Research Institute 1616 Eastlake Ave E, Suite 400, Seattle, WA, USA 98102

8 ^dCenter for Global Infectious Disease Research, Seattle Children's Research Institute, 307 Westlake
9 Avenue North, Suite 500, Seattle, USA

10 ^eLeicester School of Pharmacy, De Montfort University, Leicester, LE1 9BH, UK

11 *Corresponding author: Dr F. Brucoli.

12 E-mail: federico.brucoli@dmu.ac.uk; orcid.org/ 0000-0001-8661-2910

13 **Keywords**

14 **Abstract**

15 Antimicrobial resistance is a main concern in tuberculosis treatment and is often associated with the
16 emergence of *Mycobacterium tuberculosis* strains resistant to rifampicin (RIF), which is one of the
17 cornerstones of tuberculosis chemotherapy. In this study, aminoalkyl-aromatic ring tails were appended to
18 the C3 position of rifamycin core to assess the role of C3 substitutions to the anti-mycobacterial activity of
19 the rifamycin antibiotics. The typical hydrazone unit of RIF was replaced by an amino-alkyl linkage to
20 connect the aromatic ring tails with the rifamycin naphthoquinone core. Eight novel C3-(N-alkyl-aryl)-
21 aminoalkyl analogues of rifamycin SV were synthesised and screened *in vitro* against wild-type H37Rv
22 and “hypervirulent” HN-878 strains, and a panel of rifampicin-resistant *M. tuberculosis* clinical isolates
23 carrying mutations at the 522, 531 and 455 positions of the *rpoB* gene (RpoB_{S522L}, RpoB_{S531L} and RpoB_{H455D}
24 strains). The analogues exhibited anti-tubercular activity against H37Rv and HN-878 at submicromolar or
25 nanomolar concentrations, and against clinical H37Rv isolates bearing the S522L mutations at low
26 micromolar concentration. Benzylamine moiety-including analogue **8** was as active as rifampicin against
27 HN-878 with a MIC₉₀ value of 0.02 μ M, whereas **14** and **15**, which included tryptamine and *para*-methyl-
28 sulfonylbenzylamine C3-substituents, respectively, showed higher anti-tubercular activity (MIC₉₀ = 3 μ M)
29 compared to rifampicin against the S522L mutated H37Rv strain. Detailed *in silico* analysis of different
30 RNAP molecular systems predicted a distinct, possibly novel, binding mode for the new rifamycin
31 analogues. These were found to occupy a different space in the binding pockets of both wild type and
32 mutated RNAP proteins compared to that of rifampicin. Moreover, the molecular modelling experiments
33 investigated the ability of the novel analogues aromatic tails to establish key interactions at the RNAP

34 binding site. These interesting findings might pave the way for generating rifamycin analogues that can
35 overcome anti-microbial resistance in *M. tuberculosis*.

36 **Introduction**

37 The rifamycins are *ansa* antibiotics (ansamycins) originally isolated from fermentation cultures of
38 *Amycolatopsis rifamycinica* (previously mistakenly identified as *Streptomyces mediterranei*).^{1,2} This family
39 of bacterial secondary metabolites consists of seven molecules, rifamycins A, B, C, D, E, S and SV, which,
40 since their discovery, showed enormous potential as broad-spectrum antimicrobials and anti-tuberculosis
41 agents.^{3,4}

42 Rifamycins B (**1**) and SV (**2**) were the first members of this family to enter clinical trials as intravenous
43 antibiotics, although these compounds were found to be chemically unstable *in vivo* due their benzoquinone
44 core and showed some degrees of organ toxicity after parental administration.⁵

45 Several chemical modifications were subsequently carried out at the rifamycin C-3 side chain to produce
46 analogues with excellent sterilizing activity against *Mycobacterium tuberculosis* (*Mtb*), improved
47 PK/ADME parameters and reduced toxicity. As part of this drug development process, in the late 1960s the
48 Lepetit SPA laboratories synthesised a 3-(4-methyl-1-piperazinyl)-iminomethyl derivative of rifamycin
49 SV, rifampicin (**3**, RIF), as an orally available drug that exhibited high bactericidal activity and enhanced
50 intestinal absorption properties (**Figure 1**). RIF, which is a first-line anti-tuberculosis drug and is used in
51 combination with isoniazid, ethambutol and pyrazinamide, was marketed in Italy in 1969 and approved by
52 the FDA in USA in 1971.^{1,4} RIF is active against actively growing and non-replicating (dormant) *Mtb*
53 bacilli. However, this important anti-tubercular drug has several pitfalls, including the selection of resistant
54 mutants, if used in monotherapy, the occurrence of side effects, e.g., hepatotoxicity, and cytochrome P450
55 induction activity, which might result in drug-drug interaction issues.

56 Other rifamycins currently used in the clinic as anti-tuberculosis drugs include rifapentine (**4**, RPT) and
57 rifabutin (**5**, RBT). RPT (**4**) is an *N*-amino-*N'*-cyclopentanyl-piperazine derivative of rifamycin SV
58 developed at Lepetit SPA in the late 1960s as a long-acting version of RIF (**3**) and approved by the FDA in
59 1998.⁶ RBT (**5**) is a spiropiperidyl-rifamycin discovered by the Achifar drug company in the mid-1970s
60 that gained FDA approval in 1992 to treat *Mycobacterium avium* complex (MAC) disease in AIDS patients.
61 RBT it is also used to treat tuberculosis.⁷ RIF, RPT and RBT are on the list of WHO essential medicines.⁸
62 A number of earlier rifamycins were also investigated to treat TB, including rifalazil (KRM-1648) and 3-
63 (2,4,6-trimethylbenzylpiperazinyl)rifamycin SV (**6**, CGP-7040), although their development was
64 terminated due to either adverse side effects in patients or shortage of drug discovery funds (**Figure 1**).^{9,10,11}

65 RIF (**3**) inhibits mycobacterial transcription by binding to the β -subunit of DNA-dependent RNA
66 polymerase (RNAP). RNAP reads DNA sequences and catalyses the polymerisation of complementary
67 RNA chains using nucleotide building-blocks, thus being ultimately responsible for the transcription and
68 expression of mycobacterial genes.¹² The increase of resistance to RIF and RFB in *Mtb* is a result of
69 mutations in the 81-bp area of the *rpoB* gene, termed RIF resistance-determining region (RRDR), which
70 encodes for the β -subunit (RpoB protein) of RNA polymerase.¹³

71 Globally, in 2019 3.3% of new TB cases and 18% of previously treated cases were either multidrug- or
72 rifampicin-resistant tuberculosis (MDR/RR-TB), with an estimated 465 000 incident cases of RR-TB.¹⁴ The
73 emergence of multi-drug resistant strains and the lack of new drugs are two main factors that contribute to
74 the re-emergence of tuberculosis.

75 The RNAP core enzyme (400 kDa) consists of the five subunits: α -dimer (α_2), β subunit, β' subunit and ω ,
76 which form a holoenzyme and initiate transcription from promoters. RIF binds to the RNAP β -subunit,
77 which is located near the DNA/RNA channel, by forming hydrogen bond interactions between its four
78 hydroxyl groups at C-1, C-8, C-21, C-23 and acetoxy carbonyl oxygen at C-25, and key polymerase amino
79 acid residues.¹⁵ The C3-hydrophobic chain of RIF do not appear to be involved in crucial interactions at the
80 RNAP active site and might modulate the antibiotic activity of rifamycin derivatives by improving their
81 bacterial membrane permeation abilities.¹⁵ RIF inhibits RNAP by steric occlusion blocking the exit of the
82 growing RNA chain.¹⁶

83 Mutations at positions 526 and 531 of the RpoB protein are generally associated with high-level of RIF
84 resistance with high RIF MICs, whereas isolates bearing mutations at positions 516, 521, 522 and 533
85 exhibit moderate resistance levels to the rifamycin antibiotics RIF and RFB.^{17,18}

86 Reactions of 3-formylrifamycin SV with primary amines and amino acids¹⁹ has been attempted in the past
87 and several derivatives, which were modified at their C3 and C4 positions and contained amines, ketone,
88 hydrazine and heterocyclic moieties and sulphonium and phosphonium ylides and oximes, have been
89 prepared.²⁰⁻²⁷ However, a focussed library of rifamycin SV derivatives bearing amino alkyl-heterocyclic
90 chains at the C3 position has not been previously explored or screened for *Mtb* growth inhibition properties.
91 In earlier work, benzyl moieties have been appended to either piperazinyl unit directly linked to the C-3
92 position of the ansa macrolide core (**6**),^{9,28} or piperidyl ring attached via methylamino bridge to the
93 rifamycin SV C-3 position,²³ leading to analogues (e.g., **7**) with anti-tubercular activities against non-RR-
94 TB *Mtb* strains comparable to that of RIF.

95 Here, we sought to investigate the contributions of the hydrazone linkage and methyl-piperazinyl tail of
96 RIF to the anti-tubercular activity of the parent compound against wild-type and RR-TB *Mtb* strains. To

112 this end, a robust reductive amination protocol was devised to incorporate at the C-3 position of rifamycin
113 SV a small set of amino-alkyl aromatic/heteroaromatic rings that contained H-bond-accepting and -
114 donating groups. An aminomethyl-piperazinyl-ethanol moiety was also included at the end of the C-3 alkyl
115 tail of the macrolide to furnish a RIF-analogue (**16**) with increased hydrophilicity and a lower LogP value
116 (3.7) compared to that of parent compound **3** ($\text{LogP}_{\text{RIF}} = 4.7$) (physicochemical properties were predicted
117 using ACD Labs ACD/Phys Chem suite). The cleavable hydrazone unit of RIF was substituted with a more
118 stable, protonable, secondary amino linker, which according to previous work,²³ might increase
119 intermolecular H-bond interactions and enable rifamycin analogues to resist mycobacterial inactivation via
120 hydrolysis of their C-3 tails. As a defence mechanism against rifampicin, RIF-resistant *M. tuberculosis*
121 strains use their enzymatic armoury to hydrolyse the hydrazone unit of the ansa antibiotic²⁹ and it is
122 anticipated that the aminoalkyl linker of the novel rifamycin analogues might inhibit this inactivation
123 process. The effectiveness of the rifamycin SV derivatives against selected RR-TB strains was measured
124 using liquid, whole-cell phenotypic assays to determine minimum inhibitory concentrations (MIC_{90}).
125 Interactions of the new compounds with RIF RNAP binding site were extensively investigated using
126 molecular docking tools.

112 Chemistry

113 The reductive amination reaction of 3-formylrifamycin **7** with eight primary alkyl(aromatic) amines was
114 carried out in a parallel synthetic fashion using sodium triacetoxyborohydride [$\text{NaBH}(\text{OAc})_3$] as a mild and
115 selective reducing agent (**Scheme 1**). Previous reductive amination attempts on the same substrate using
116 sodium cyanoborohydride (NaBH_3CN) resulted in lower-yielding, slower and less clean reactions
117 compared to $\text{NaBH}(\text{OAc})_3$ and therefore NaBH_3CN was not further pursued as the reducing agent.

118 The reactions proceeded smoothly, and the title compounds (**8-16**) were produced in medium to high yield.
119 The presence of a protonated nitrogen atom at the C-38 position was corroborated by NMR analysis, as can
120 be noted in the proton spectrum of **8** (**Figure 2a**). This confirmed previous findings that C-3 amino linked
121 rifamycin conjugates undergo intramolecular zwitterionisation as a result of proton transfer between the
122 acidic naphthoquinone C-8-OH and C-38-nitrogen in protic solvents or in the presence of water.^{30,31}

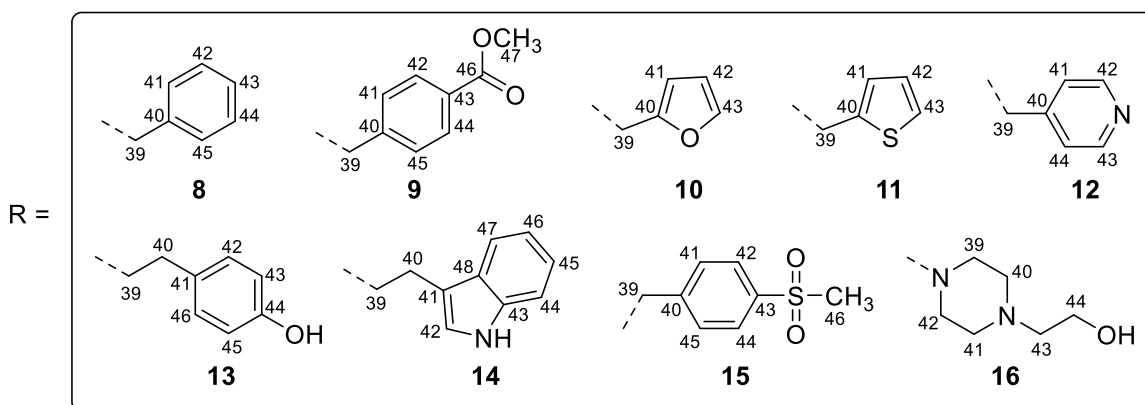
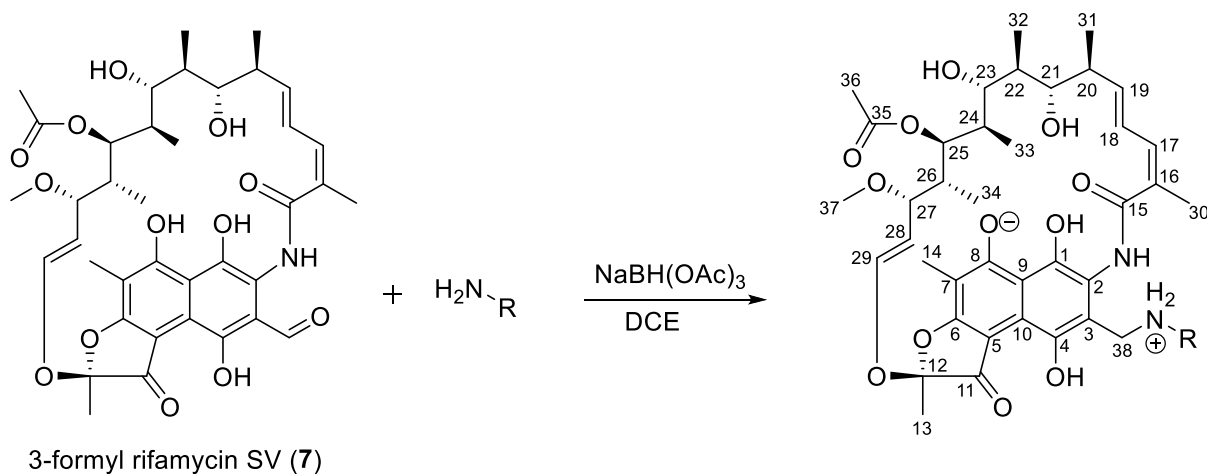
123 The structure assignment of carbon and proton nuclei of derivative **8** are illustrated in the ^1H - ^{13}C HSQC
124 spectrum of **Figure 2b**, **Table S1** and **Figure S1** (HMBC spectrum).

125 Strains RRDR mutations analysis and antitubercular activity evaluation

126 The *rpoB* gene of the 65 RR-isolates examined in this study was successfully sequenced from codon 507
127 through 533 to identify clinically relevant mutations (**Table 1**). The most frequent mutation (41%) in the
128 RpoB RRDR was found to be at the 531 position, with 18 isolates bearing the S531L mutations (serine

129 replaced by leucine). The second most frequent mutation (40%) was at position 526, with 12 isolates
 130 carrying the H526D (histidine replaced by aspartic acid). A relevant number of isolates also possessed the
 131 S522L (9%) mutation.

132



133

134 **Scheme 1.** Synthesis of rifamycin analogues **8-16**. Reagents and conditions: amines (1 equiv.),
 135 $\text{NaBH}(\text{OAc})_3$ (1.4 equiv.), dichloroethane (DCE, 5 mL), room temperature, 3 h, 55-83% yield.

136 The novel rifamycin derivatives were screened for whole-cell growth inhibition of *M. tuberculosis* H37Rv
 137 and HN878 wild-type strains, and RR-resistant strains RpoB_{S522L} RpoB_{S531L} and RpoB_{H455D} (HN-0258218-
 138 RM1), which was isolated as a spontaneous rifampicin resistant mutant from HN-878,³² and minimum
 139 inhibitory concentrations (MICs) were determined at five days (**Table 2**). The “hypervirulent” *Mtb* HN878
 140 was selected as it is a particularly insidious strain due to its ability to grow fast and drastically reduce the
 141 survival rate of immune-competent infected mice.³³ RIF-resistant strains with S531L and S522L mutations
 142 were chosen as they are generally found in isolates from a high proportion of MDR-TB patients.¹⁷

143 **Table 1.** Sequencing of the *rpoB* gene of Rif-resistant-isolates used in this study including the numbering of the residues from the crystal structure of RNAP
 144 in complex with rifampicin (PDB ID 5UHC).³⁴ The mutations that confer RR-resistance in *Mtb* are shown below the amino acid sequence of the rpoB protein.
 145 In brackets are indicated the number of isolates carrying a specific single amino acid mutation in the RNAP β -subunit.

Position	507	508	509	510	511	512	513	514	515	516	517	518	519	520	521	522	523	524	525	526	527	528	529	530	531	532	533
Position (5UHC)	432	433	434	435	436	437	438	439	440	441	442	443	444	445	446	447	448	449	450	451	452	453	454	455	456	457	458
Codons	GGC	ACC	AGC	CAG	CTG	AGC	CAA	TTC	ATG	GAC	CAG	AAC	AAC	CCG	CTG	AGC	GGC	TTG	ACC	CAC	AAG	CGC	CGA	CTG	TCG	CGC	CTG
Aminoacids	G	T	S	Q	L	S	Q	F	M	D	Q	N	N	P	L	S	G	L	T	H	K	R	R	L	S	A	L
Mutations	G (1)				P (1)		K (1)			G (1)		Y (1)			L (6)				D (12)						L (18)		
	D (1)									Y (1)									L (6)						W (5)		
										V (1)										Y (3)					Q (1)		
																				R (1)					Y (1)		
																				P (1)							
																				N (1)							
																				A (1)							

146

147

148

149 **Table 2.** Minimum inhibitory concentrations (MICs) of **8-16** in *M. tuberculosis* H37Rv, HN-878 and
 150 rifampicin resistant strains RpoB_{S522L}, RpoB_{S531L} and RpoB_{H455D} isolated from HN-878.

<i>Mycobacterium tuberculosis</i> strains MIC ₉₀ (μM) ^a						
Cmp ID	H37Rv-LP ^b	HN-878 ^c	RpoB _{S522L} H37Rv ^d	RpoB _{S531L} ^e	RpoB _{H455D} ^f	
8	0.097 ± 0.041	0.026 ± 0.035	12	> 20	9.9	
9	0.12 ± 0.046	0.53 ± 0.064	7.7	> 20	> 20	
10	0.090 ± 0.028	0.45 ± 0.140	> 20	> 20	16	
11	0.082 ± 0.021	0.20 ± 0.057	8	> 20	14	
12	0.075 ± 0.021	0.31 ± 0.140	6.7	> 20	> 20	
13	0.066 ± 0.019	0.22 ± 0.045	5.8	> 20	> 20	
14	0.039 ± 0.060	0.39 ± 0.010	3.1	> 20	> 20	
15	0.039 ± 0.046	0.096 ± 0.064	3.2	> 20	> 20	
16	0.034 ± 0.028	0.070 ± 0.042	4.7	> 20	> 20	
RIF (3)	0.0045	0.02	> 8.0	> 8.0	> 8.0	
Isoniazid	0.28	0.29	0.29	0.55	0.62	

151 [^a] MIC₉₀ was defined as the concentration required to inhibit growth of *M. tuberculosis* in liquid medium
 152 by 90% after 5 days. [^b] H37Rv (ATCC 25618 Wild-type). [^c] HN-878 wild-type. [^d] (RIF-R1) Rifampicin-
 153 resistant strain (RpoB_{S522L} H37Rv-LP). [^e] (RIF-R2) Rifampicin-resistant strain (RpoB_{S531L}). [^f] (HN-
 154 0258218-RM1) Rifampicin-resistant strain (RpoB_{H455D}) isolated from HN-878. The screening was
 155 conducted in triplicate.

156
 157 The new rifamycin analogues **8-16** were active against *Mtb* H37Rv, HN-878 and RpoB_{S522} RIF-resistant
 158 strains, but not against the RpoB_{S531L} RR-strain. *Mtb* H37Rv was found to be the most susceptible strain to
 159 the anti-tubercular activity of the compounds. Analogues **8**, **11**, **12**, **13**, **15**, **14** and **16** exhibited significant
 160 growth inhibitory properties against H37Rv with MIC values ranging from 0.034-0.097 μM, albeit with a
 161 7- to 20-fold reduced potency compared to RIF (MIC = 0.0045 μM). Compounds **9** was only active at a
 162 concentration of 0.12 ± 0.046 μM, indicating that hydrogen bond acceptor groups, e.g., methyl carboxylate
 163 unit, are not well tolerated in the RNAP_{H37Rv} binding pocket.

164 Benzylamino residue-containing analogue **8** was as effective as RIF (**3**) in killing the hypervirulent strain
 165 HN-878 with a MIC₉₀ value of 0.026 ± 0.035 μM. Rifamycin derivatives **9**, **10**, **11**, **12**, **13** and **14** were less
 166 active against HN-878 compared to **8** with MIC₉₀ ranging from 0.20-0.53 μM. Compounds **15** and **16**
 167 arrested the growth of HN-878 at concentrations of 0.096 ± 0.064 and 0.070 ± 0.042 μM, respectively.
 168 Compounds **8**, **10** and **11** were active, albeit at higher concentrations (9-16 μM), against the RR strain
 169 (RpoB_{H455D}) isolated from HN-878.

171 The title compounds **8-16** inhibited the growth of *Mtb* RpoB_{S522L} with MIC values ranging from 3-12 μ M.
 172 Notably, analogues **14** and **15**, which contained tryptamine and methylsulfonyl-benzylamine residues,
 173 respectively, exhibited cidal activity against *Mtb* RpoB_{S522L} at a concentration as low as 3.1-3.2 μ M,
 174 whereas RIF was not effective against this strain (MIC >8 μ M).

175

176 Molecular modelling studies

177 Docking studies were carried out to evaluate the binding mode of the RIF-analogues and investigate the
 178 interactions of the compounds' functional groups, including their amino-methyl aromatic tails or
 179 aminomethyl-piperazinyl-ethanol moiety (**16**), with the amino acid residues in the binding pockets of the
 180 β -subunits of wild-type (PDB ID 5UHC),³⁴ and S531L- and S522L-mutated RNAP enzymes. The optimised
 181 3D structures of rifampicin analogues were docked into the RNAP binding site defined by the location of
 182 rifampicin in the complex. The resulting docking scores of the zwitterionic analogues (**Table 3**) indicated
 183 favourable interactions between the analogues and the amino acid residues of the RNAP. Although there is
 184 no direct correlation between the docking score and MICs of the majority of tested molecules, the molecular
 185 docking has revealed possible a novel mode of binding for the rifampicin analogues.

186 **Table 3.** Docking scores (kcal/mol) of zwitterionic **8-16** against *M. tuberculosis* H37Rv RpoB and
 187 rifampicin resistant strains RpoB_{S522L} and RpoB_{S531L} as targets. The docking scores were predicted using
 188 LeDock software. The docking score in brackets correspond to second pose.

Cmp ID	RpoB H37Rv whole system ^[a]	RpoB H37Rv whole system (10 ns simulated)	RpoB H37Rv β -subunit (10 ns simulated)	RpoB _{S531L} H37Rv whole system (50 ns simulated)	RpoB _{S522L} H37Rv β -subunit (150 ns simulated)
8	-7.9	-8.5	-6.5	-7.2	-6.8
9	-8.7	-9.2	-6.9	-8.3	-7.6
10	-7.9	-8.4	-6.4	-7.2	-6.8
11	-8.1	-8.8	-6.0	-7.4	-7.1
12	-7.8	-8.7	-6.7	-7.5	-7.0
13	-7.9	-8.7	-6.6	-7.4	-6.9
14	-8.7	-9.5	-7.4	-8.6	-7.7 (-7.7)
15	-8.5	-9.5	-7.1	-8.2	-7.8 (-7.3)
16	-7.0 (-6.8)	-9.8	-6.5	-7.9	-7.4
RIF (3)	-7.1	-8.7	-6.1	-7.4	-6.5

189 ^[a] wild type protein PDB ID 5UHC (system was not simulated prior to docking). ^[b] Binding score for the
 190 second pose.

191 Molecular docking of the analogues into the rifampicin binding pocket of the wild type RNAP crystal
 192 structure (PDB ID 5UHC) indicated a possibility of three distinct modes of their interaction with RNAP

193 (Figure S2a-d). Most of the analogues occupied the same space as rifampicin, with their cores overlapping
194 with rifampicin core and different position of their tails (Figure 3a). Consequently, these analogues form
195 interactions with the key residues in WT RNAP similar to those observed for rifampicin.³⁴ In particular,
196 hydrogen bonds were observed between those analogues and amino acids Q435, Q438, R454 and S456.
197 Analogues 15 has a possibility to form additional hydrogen bond interactions with nucleotide and G491
198 (Figure 3a).

199 Analogues 12 and 13 partially occupied the cavity with their core occupying the similar space as the
200 rifampicin tail (Figure S2b). These analogues do not form the hydrogen bonds with the same residues
201 despite being in close proximity, but their binding poses are stabilised by forming hydrogen bonds with
202 R173 and F439 and via interactions with hydrophobic residue I497. While the most favourable pose of 16
203 partially occupied the RNAP binding site (Figure S2c), the second pose occupied a similar space as
204 rifampicin (Figure S2d). Furthermore, some of the less favourable docking poses of other analogues were
205 adopting conformations that are less deviating from the rifampicin binding mode.

206 There is a lack of direct correlation between the docking scores and experimentally observed activities
207 (Tables 1 and 3), that may be due not only to different space of the binding site the ligands occupy when
208 compared to rifampicin, but also due to their multiple conformations that can be formed within the binding
209 site (Figure S4). While rifampicin forms fewer conformations with one preferred, its analogues can form
210 between 7 to 13 conformations, and some are unlike to be bioactive. As the binding scores can be very
211 similar, the probability of having both bioactive and inactive conformations are high, which could be one
212 of the reasons for the lower activities of rifampicin analogues. The higher number of possible binding modes
213 most likely results from introduction of rotatable bonds in the tails, thus increasing the flexibility of
214 analogues. The number of torsion angles that can be changed increased from 5 in rifampicin to either 7, 8
215 or 9. Additionally, the higher predicted logP and lower predicted solubility of analogues, which are reflected
216 in lower predicted drug likeness, when compared to rifampicin, may also contribute to lower biological
217 activity (Table S2). Additionally, these difference in molecular properties may also affect the permeability
218 of the analogues as demonstrated for a different set of rifampicin analogues.³⁰

219 Notably, rifampicin and analogues did not fully occupy the available space inside the binding site, and one
220 of the pockets at the bottom of the cleft may be explored by the analogues (Figure S2b). Since the protein,
221 DNA and RNA conformations from the crystal structure may lead to biased docking results, a short
222 molecular dynamics simulation was conducted to relax the 3D structure of the whole system. The docking
223 of all analogues against the 3D structure extracted from the final frame of the trajectory has resulted in the
224 docking poses that had considerable higher docking score. The careful analysis of the results indicated that
225 the shape of the binding cavity was changed due to the change of RNA chain conformation and shrinking

226 the space available for ligand binding. This resulted in rifampicin and all analogues interacting mainly with
227 the RNA chain and therefore providing potentially misleading information.

228 Therefore, the binding of analogues with the protein only was explored by considering the 3D structure of
229 the beta subunit on its own, an approach that was previously reported elsewhere.³⁵ Consequently, the
230 structure of the beta subunit and rifampicin complex was extracted from the crystal structure file³⁴ and
231 subjected to a 10 ns molecular dynamics simulation of a partially restrained protein chain that was more
232 than 10 Å away from the rifampicin as a preparation of the protein structure for the docking. Similar to
233 results of the docking against the whole RNAP, different binding modes were observed. The first pose of
234 The cores of **9** and **11** occupied the similar space as rifampicin (**Figure S3a**), while most analogues had
235 their tails occupying previously unexplored space of the binding site (pocket marked with a red circle) that
236 can be seen on the bottom left of **Figure S2b**. Their cores (except **16**) did not occupy the similar space as
237 the rifampicin and have formed set of interactions with a new residue within previously unoccupied space
238 of the RNAP binding site, namely T488 (**Figure 4a**).

239 Finally, the reasons behind a diminished anti-tubercular activity of the analogues due to S531L mutation
240 were explored *in silico* by replacing the serine side chain with a leucine residue at 456 position in the PDB
241 file with RNAP crystal structure (PDB ID 5UHC).³⁴ The 50 ns molecular dynamics simulation was
242 conducted on the modified protein and the final frame of the trajectory was used as a target in the additional
243 docking experiments. Albeit the docking scores are lower when compared to those obtained for the wild
244 type protein, these cannot provide explanation for the complete loss activity of these analogues and
245 rifampicin. However, the shape of the binding site in the wild type protein appears considerably deeper than
246 the putative binding site in the mutated protein (**Figure 5a-b**). Interestingly, it can be observed that
247 introduction of the leucine instead of serine changes the conformation on surrounding hydrophobic residues
248 (V176, L458 and I497 in **Figure 5b**). These changes not only lead to modifications to the volume, but also
249 have a profound effect on the hydrophobicity of the cleft. This, in turn, has potentially a significant effect
250 on ligand binding and can provide a structural information regarding the lack of activity against this
251 particularly resistant strain.

252 Moreover, the change of the binding site shape in the protein with S522L mutation may explain the loss of
253 anti-tubercular activity of rifampicin (**3**), the different range of activities displayed by most analogues and
254 the increased efficacy of **15** (**Figure 5c**). As the S522 (position 447 in 5UHC) is not part of the binding site,
255 a longer molecular dynamics simulation of the mutated beta subunit was conducted, which revealed that
256 the larger leucine side chain displaced nearby binding site residues (**Figure 5d**). In particular, R454 and
257 R613 were displaced when compared to their locations in the crystal structure,³⁴ thus preventing formation
258 of favourable interactions and resulting in the loss of activity of **3**. This is indicated to some extent by lower

259 binding scores obtained for rifampicin docked against the binding site of wild type beta subunit (-8.7
260 kcal/mol) and S522L mutated beta protein (-7.4 kcal/mol) (**Table 3**). On the contrary, most of analogues
261 retained their activity, which may be a result of their potentially different binding modes, due to their C3-
262 aromatic tails, when compared to rifampicin. Interestingly, in addition to previously explored binding site
263 space, tails of two most potent analogues were found to bind into a previously unoccupied space in the
264 second most favourable poses. As illustrated in **Figure 6a**, the aromatic tails of **14** and **15** nicely fitted into
265 the space of the S522L mutated beta protein showing a favourable docking scores of -8.6 and -8.2 kcal/mol,
266 respectively. These scores somewhat correlated with the compounds' MIC₉₀ values (3.1 and 3.2 μM,
267 respectively), which was one of the lowest of the series against RpoB_{S522L} H37Rv.

268 These computational investigations indicate a possible rationale for the loss of rifampicin activity against
269 resistant strains based on the changes of the binding site space as a result of amino acid mutations near the
270 active site. However, further extended molecular dynamics simulations or crystallographic studies would
271 be needed to confirm the exact nature of the protein structure changes resulting from the mutations of the
272 residues that are not part of the binding site. Importantly, insights into putative mechanism of action of the
273 rifampicin analogues were revealed and opened opportunities for optimising the activity of RNAP
274 inhibitors. These studies provide a basis for further computer aided molecular design by targeting space
275 previously unoccupied by rifampicin.

276

277 **Conclusions**

278 Mutations in *M. tuberculosis* (*Mtb*) drug targets are one of the main hurdles preventing effective treatment
279 and management of the tuberculosis disease. Mutations in the *rpoB* gene encoding for the β-subunit of
280 DNA-dependent RNA polymerase (RNAP) lead to an increased resistance in *Mtb* to rifamycin antibiotics,
281 such as rifampicin (**3**), a first-line drug widely used for tuberculosis treatment. Extensive SAR studies
282 previously demonstrated that the naphthoquinone core and hydroxyl groups attached to the aliphatic
283 ansa bridge of rifampicin are essential pharmacophoric characteristics enabling tight contacts with key
284 amino acids in the RNAP β-subunit binding site. On the other hand, the 4-methyl-1-piperazinyl-
285 iminomethyl unit of rifampicin might have a less prevalent role in establishing interactions with the binding
286 pocket, although several authors reported different, sometimes contrasting, viewpoints on the ability of the
287 rifampicin tail to form interactions with key residue E445 in the RNAP site.^{20,23,27} It was therefore postulated
288 that structurally diverse C3-RIF tails did not affect ligand-protein interactions but might improve DM/PK
289 of the molecules and alter permeability of bacterial cell walls instead, leading to RIF variants with different
290 bactericidal activity.³⁶

291 Here, in an effort to explore the contribution of C-3 tails to the anti-tubercular activities and ligand binding
292 properties of rifamycin analogues, the piperazinyl-iminomethyl unit of rifampicin (**3**) was replaced with
293 eight amino-alkyl-aromatic rings. The latter were connected to the naphthoquinone chromophore with a
294 stable secondary amino linker, which in turn replaced RIF's cleavable hydrazone linkage. The resulting
295 novel C3-(*N*-alkyl-aryl)-aminomethyl rifamycin analogues were screened against *M. tuberculosis* H37Rv
296 and HN-878 strains, and clinical isolates bearing 522, 531 and 455 mutations. Interestingly, it was found
297 that benzylamino-including analogue **8** was as effective as RIF (**3**) in inhibiting the growth of the
298 hypervirulent HN-878 strain with a MIC₉₀ value of 0.02 μM. The RpoB_{H455D} HN-878 strain bearing a
299 mutation outside the hotspot region of *rpoB* gene was also sensitive to compound **8**. Moreover, tryptamine-
300 and methyl-sulfonyl-benzyl-containing analogues **14** and **15**, respectively, were found to be active against
301 RpoB_{S522L} H37Rv (MIC₉₀ = 3 μM), whilst RIF was not effective against this strain. The S522L mutation
302 has a high incidence in *Mtb* clinical isolates, and the scaffold of rifamycin derivatives active against strains
303 bearing this mutation might be used for the development of more effective anti-tubercular agents.

304 *In silico* docking studies provided a possible rationale for the anti-tubercular activity of the novel analogues,
305 which might have alternative modes of ligand interactions with the RNAP subunit. Moreover, the docking
306 results showed that the analogues' aromatic tails might play a more prominent role in establishing molecular
307 interactions within the binding site compared to RIF piperazine unit. Our molecular modelling experiments
308 revealed novel binding pockets within the β-subunit that can be chemically explored by *ad hoc* designed
309 rifampicin analogues. For example, the aromatic tails of some analogues, including **14** and **15**, were found
310 to be positioned in a space of RpoB_{S531L} binding site that was not occupied by the rifampicin piperazine
311 moiety. Also, it was noted that the binding site of the RpoB_{S531L} mutant strain was narrower compared to
312 the one of the H37Rv RpoB protein, this probably occurring as direct result of the substitution of a serine
313 with a leucine residue. In summary, this study offers an insight in the design of more active class of RIF-
314 based anti-TB agents and highlights the role of selected C-3 appended aromatic tails in increasing the
315 molecular interactions of rifamycin analogues with amino acid residues of the RNAP β subunit. These
316 results might also serve as a basis for further computational studies to explain effects of other mutations on
317 rifampicin derivatives activities.

318

319 **Experimental**

320 **General Chemistry Information**

321 ¹H and ¹³C Nuclear Magnetic Resonance (NMR) spectroscopy analyses were carried out using a JEOL
322 JNM-ECZR 600 MHz (equipped with a ROYAL probe) or Bruker Avance 400 MHz NMR spectrometers.

323 Solvent signals for hydrogen and carbon NMR were used as the internal reference. Chemical shifts (δ_{H}) are
324 quoted in parts per million and are relative to the solvents residual peaks in the ^1H and ^{13}C NMR spectra:
325 CDCl_3 (7.26 and 77.0 ppm), $\text{MeOD-}d_4$ (3.31 and 49.1 ppm) and $\text{DMSO-}d_6$ (2.50 and 39.52 ppm). Coupling
326 constants (J) are given in Hertz (Hz) and the signal multiplicity is described as singlet (s), doublet (d),
327 doublet of doublets (dd), triplet of doublets (td), triplet (t), quartet (q) and multiplet (m). Chemicals were
328 purchased from Acros Organic, Alfa Aesar, Fisher Scientific, Sigma Aldrich and VWR. The deuterated
329 solvents (CDCl_3 , $\text{DMSO-}d_6$ and $\text{MeOD-}d_4$) used for NMR spectroscopy experiments were purchased from
330 Cambridge Isotope Laboratories Inc. Thin Layer Chromatography (TLC) was performed using aluminium
331 backed 20×20 cm silica gel 60 F₂₅₄, which were purchased from Merck for viewing colourless spots under
332 254 nm wavelength ultraviolet light. Flash column chromatography purifications of the intermediates and
333 final products were conducted in a glass column using irregular, 60 Å pore size silica gel, 63-200 μm , 70-
334 230 mesh. LC-MS analysis was conducted on a Thermo Fisher – Agilent 6100 series Quadrupole LC-MS
335 system with a G4220A 1290 binary pump/DAD. The column used was an Agilent Zorbax SB-C19 2.1 \times
336 50 mm 1.8 micron (400 bar). Parallel synthesis was carried out using Radleys Carousel 12 Plus reaction
337 station.

338 Reductive amination procedure

339 The aromatic primary amine (1 equiv.) was added to a solution of rifaldehyde **7** (0.1 mmol, 72.6 mg) in
340 1,2-dichloroethane (10 mL) and subsequently treated with sodium triacetoxyborohydride (1.4 equiv., 29.7
341 mg). The mixture was stirred at room temperature for 2 hours under nitrogen atmosphere. After HPLC
342 analysis showed consumption of the starting material, the reaction was quenched with 10% NaHCO_3 (10
343 mL) and the compounds extracted with EtOAc (3×15 mL). The organic phase was dried with MgSO_4 and
344 the solvent was evaporated under reduced pressure to yield the free base as a crude reddish residue, which
345 was purified by column chromatography using a Hexane: EtOAc /1:9 solvent system.

346 **8**. A red solid (45 mg, 55%) $R_f = 0.34$ ($\text{EtOAc} - \text{MeOH}$ 100:1 v/v); MS m/z 817.4 (M^+); $^1\text{H-NMR}$ (600
347 MHz, $\text{DMSO-}d_6$) δ_{H} 9.27 (s, 1H, NH-amide), 8.93 (s, 1H, NH-amine), 8.55 (s, 1H, NH-amine), 7.49-7.48
348 (m, 2H, H-41/45), 7.37-7.36 (m, 3H, H-42/44, H-43), 6.40-6.36 (m, 1H, H-18), 6.27-6.26 (m, 1H, H-17),
349 6.26-6.24 (m, 1H, H-29), 6.02 (dd, J = 15.9, 7.5 Hz, 1H, H-19), 5.06 (d, J = 11.1 Hz, 1H, H-25), 4.90 (dd,
350 J = 12.8, 8.5 Hz, 1H, H-28), 4.25-4.23 (m, 1H, H-38), 4.19 (s, 2H, H-39), 3.92 (d, J = 9.0 Hz, 1H, C-23-
351 OH), 3.57-3.55 (m, 2H, H-21, H-38), 3.22 (d, J = 8.7 Hz, 1H, H-27), 2.87 (s, 3H, H-37), 2.81-2.77 (m, 1H,
352 H-23), 2.25-2.21 (m, 1H, H-20), 1.97 (s, 3H, H-36), 1.94 (s, 3H, H-30), 1.91 (s, 3H, H-14), 1.65 (s, 3H, H-
353 13), 1.61-1.60 (m, 1H, H-22), 1.20-1.17 (m, 1H, H-24), 0.96-0.93 (m, 1H, H-26), 0.89 (d, J = 7.0 Hz, 3H,
354 H-32), 0.78 (d, J = 7.0 Hz, 3H, H-31), 0.39 (d, J = 6.9 Hz, 3H, H-33), -0.38 (d, J = 6.8 Hz, 3H, H-34); $^{13}\text{C-}$
355 NMR (151 MHz, $\text{DMSO-}d_6$) δ_{C} 185.3 (C-11), 180.1 (C-8), 172.0 (C-6), 169.9 (C-15), 169.4 (C-35), 151.4

356 (C-1), 145.0 (C-4), 142.1 (C-29), 140.4 (C-19), 137.2 (C-40), 135.3 (C-17), 131.0 (C-16), 129.8 (C-41/45),
357 128.7 (C-42/44), 126.3 (C-18), 119.0 (C-2), 118.2 (C-28), 118.0 (C-10), 117.6 (C-9), 113.8 (C-3), 108.8
358 (C-12), 100.4 (C-7), 98.6 (C-5), 77.0 (C-27), 75.7 (C-23), 71.2 (C-25), 70.4 (C-21), 55.6 (C-37), 42.1 (C-
359 38), 41.7 (C-39), 40.2 (C-26), 38.1 (C-24), 37.8 (C-20), 32.6 (C-22), 22.1 (C-13), 20.7 (C-36), 19.9 (C-30),
360 18.2 (C-31), 11.1 (C-32), 9.0 (C-34), 8.6 (C-33), 7.4 (C-14); HRMS: found 816.3838, calculated for
361 $C_{45}H_{56}N_2O_{12}$ 816.3833.

362 **9.** A red solid (59 mg, 65%) $R_f = 0.25$ (EtOAc - MeOH 100:1 v/v); MS m/z 875.5 (M^+); 1H -NMR (400
363 MHz, DMSO- d_6) δ_H 9.22 (s, 1H), 9.09 (s, 1H), 8.54 (s, 1H), 7.91 (d, $J = 8.4$ Hz, 2H), 7.64 (d, $J = 8.1$ Hz,
364 2H), 6.52 (d, $J = 3.1$ Hz, 1H), 6.28-6.24 (m, 1H), 6.18 (d, $J = 12.4$ Hz, 1H), 5.96 (q, $J = 7.5$ Hz, 1H), 5.05
365 (d, $J = 11.5$ Hz, 1H), 4.91 (dd, $J = 12.9, 8.1$ Hz, 1H), 4.33 (bs, 2H), 4.23-4.19 (m, 1H), 4.00 (d, $J = 8.3$ Hz,
366 1H), 3.91 (s, 3H), 3.58-3.55 (m, 1H), 3.24-3.22 (m, 1H), 2.95 (s, 1H), 2.88 (s, 3H), 2.79 (t, $J = 7.4$ Hz, 1H),
367 2.22-2.20 (m, 1H), 1.97 (s, 3H), 1.91 (s, 3H), 1.65 (s, 3H), 1.62 (s, 3H), 1.23 (bs, 1H), 0.88 (d, $J = 7.1$ Hz,
368 3H), 0.84 (d, $J = 7.4$ Hz, 3H), 0.42 (d, $J = 7.1$ Hz, 3H), -0.37 (d, $J = 6.8$ Hz, 3H); HRMS: found 874.3888,
369 calculated for $C_{47}H_{58}N_2O_{14}$ 874.3880.

370 **10.** A red solid (60 mg, 70%) $R_f = 0.29$ (EtOAc - MeOH 100:1 v/v); MS m/z 807.1 (M^+); 1H -NMR (600
371 MHz, DMSO- d_6) δ_H 9.27 (s, 1H), 9.01 (s, 1H), 8.57 (s, 1H), 7.67 (d, $J = 1.4$ Hz, 1H), 6.60 (d, $J = 3.4$ Hz,
372 1H), 6.53-6.49 (m, 1H), 6.46 (q, $J = 1.6$ Hz, 1H), 6.29 (d, $J = 10.3$ Hz, 1H), 6.25 (d, $J = 12.4$ Hz, 1H), 6.06
373 (q, $J = 7.8$ Hz, 1H), 5.07 (d, $J = 11.7$ Hz, 1H), 4.90 (dd, $J = 13.1, 8.3$ Hz, 1H), 4.36-4.32 (m, 1H), 4.24-4.20
374 (m, 2H), 3.95 (d, $J = 8.3$ Hz, 1H), 3.69-3.64 (m, 1H), 3.23 (d, $J = 9.0$ Hz, 1H), 2.94 (s, 1H), 2.88 (s, 3H),
375 2.81 (t, $J = 7.9$ Hz, 1H), 2.27 (q, $J = 7.8$ Hz, 1H), 1.98 (d, $J = 4.1$ Hz, 3H), 1.93 (s, 3H), 1.91 (d, $J = 3.4$ Hz,
376 3H), 1.65 (s, 3H), 1.61 (s, 1H), 1.23 (s, 1H), 0.91 (d, $J = 6.9$ Hz, 3H), 0.86 (d, $J = 6.9$ Hz, 3H), 0.46 (d, $J =$
377 6.9 Hz, 3H), -0.36 (d, $J = 6.9$ Hz, 3H); ^{13}C -NMR (151 MHz, DMSO- d_6) δ_C 186.9, 184.0, 174.1, 171.4,
378 167.4, 154.4, 148.7, 145.3, 144.8, 143.1, 140.2, 139.2, 137.7, 131.7, 130.9, 130.1, 128.0, 126.4, 126.2,
379 123.0, 120.5, 116.6, 115.1, 112.5, 111.0, 108.8, 98.6, 77.9, 76.2, 73.1, 73.0, 55.6, 49.4, 42.7, 40.9, 40.2,
380 37.9, 37.4, 33.8, 22.0, 20.7, 19.8, 18.1, 11.1, 9.0, 8.7, 7.3; HRMS: found 806.3630, calculated for
381 $C_{43}H_{54}N_2O_{13}$ 806.3626.

382 **11.** A red solid (72 mg, 78%) $R_f = 0.33$ (EtOAc - MeOH 100:1 v/v); MS m/z 823.4 (M^+); 1H -NMR (600
383 MHz, DMSO- d_6) δ_H 9.23 (s, 1H), 7.62-7.58 (m, 1H), 7.26 (d, $J = 12.1$ Hz, 1H), 7.21 (d, $J = 11.4$ Hz, 1H),
384 6.49 (d, $J = 23.8$ Hz, 1H), 6.45 (dd, $J = 15.5, 11.4$ Hz, 0H), 6.28 (d, $J = 12.7$ Hz, 1H), 6.24 (d, $J = 12.7$ Hz,
385 1H), 6.04 (q, $J = 7.8$ Hz, 1H), 5.07 (d, $J = 11.0$ Hz, 1H), 4.91 (dd, $J = 12.7, 8.3$ Hz, 0H), 4.45-4.37 (m, 1H),
386 4.25-4.20 (m, 1H), 4.03 (q, $J = 7.1$ Hz, 1H), 3.94 (d, $J = 9.0$ Hz, 0H), 3.63 (d, $J = 12.1$ Hz, 1H), 3.25-3.23
387 (m, 1H), 2.89 (d, $J = 4.8$ Hz, 3H), 2.82-2.79 (m, 0H), 2.27-2.22 (m, 1H), 1.98 (d, $J = 6.4$ Hz, 3H), 1.95 (s,
388 3H), 1.91-1.91 (m, 3H), 1.64 (d, $J = 3.4$ Hz, 3H), 1.63 (s, 1H), 1.25-1.22 (m, 1H), 0.91 (d, $J = 6.5$ Hz, 3H),

389 0.83 (d, J = 6.5 Hz, 3H), 0.42 (d, J = 6.9 Hz, 3H), -0.36 (d, J = 6.9 Hz, 3H); ¹³C-NMR (151 MHz, DMSO-
390 *d*₆) δ_C 185.1, 184.5, 172.3, 171.0, 169.6, 167.6, 149.0, 145.2, 143.3, 137.9, 135.0, 133.0, 132.3, 131.6,
391 128.6, 127.6, 117.7, 117.4, 116.9, 116.4, 113.8, 109.1, 108.4, 98.8, 76.6, 76.0, 73.1, 72.9, 60.0, 55.9, 42.5,
392 40.9, 40.3, 38.1, 37.2, 22.3, 20.9, 20.3, 18.4, 11.3, 8.9, 8.5, 7.6; HRMS: found 822.3392, calculated for
393 C₄₃H₅₄N₂O₁₂S 822.3397.

394 **12.** A red solid (65 mg, 79%) *R*_f = 0.25 (EtOAc - MeOH 100:1 v/v); MS *m/z* 818.3 (M⁺1); ¹H-NMR (600
395 MHz, DMSO-*d*₆) δ_H 9.24 (s, 1H), 8.74 (s, 1H), 8.61 (d, J = 5.5 Hz, 1H), 8.56 (d, J = 5.5 Hz, 2H), 7.48-7.51
396 (2H), 6.51 (s, 2H), 6.27 (s, 1H), 6.24 (s, 1H), 6.02 (q, J = 7.8 Hz, 1H), 5.09 (d, J = 3.8 Hz, 1H), 5.06 (d, J =
397 11.0 Hz, 1H), 4.97 (q, J = 5.5 Hz, 1H), 4.26 (s, 1H), 3.93 (d, J = 9.0 Hz, 1H), 3.58 (d, J = 12.1 Hz, 2H),
398 3.23 (d, J = 9.0 Hz, 1H), 3.14 (d, J = 10.3 Hz, 1H), 3.08 (d, J = 10.0 Hz, 1H), 2.88 (s, 3H), 2.82-2.78 (m,
399 1H), 2.25-2.20 (m, 1H), 1.99 (s, 3H), 1.98 (s, 3H), 1.91 (s, 3H), 1.65 (s, 3H), 1.23 (s, 1H), 0.90 (s, 3H), 0.88
400 (d, J = 3.8 Hz, 3H), 0.76 (d, J = 6.9 Hz, 3H), 0.42 (d, J = 6.9 Hz, 3H), -0.36 (d, J = 6.9 Hz, 3H); ¹³C-NMR
401 (151 MHz, DMSO-*d*₆) δ_C 186.5, 183.4, 171.8, 170.8, 169.3, 150.0, 144.0, 143.0, 139.8, 139.0, 138.8, 131.9,
402 131.7, 130.9, 128.1, 126.3, 125.9, 124.2, 119.4, 117.9, 114.5, 108.8, 102.3, 76.3, 75.2, 73.1, 73.0, 55.6,
403 43.0, 40.0, 38.1, 32.5, 22.0, 20.6, 20.0, 19.8, 18.1, 11.0, 8.9, 8.6, 7.3. HRMS: found 817.3781, calculated
404 for C₄₄H₅₅N₃O₁₂ 817.3786.

405 **13.** A dark red solid (68 mg, 81%) *R*_f = 0.31 (EtOAc - MeOH 100:1 v/v); MS *m/z* 847.3 (M⁺1); ¹H-NMR
406 (600 MHz, DMSO-*d*₆) δ_H 9.28 (s, 1H), 8.40 (s, 1H), 8.27 (s, 1H), 7.02-7.00 (m, 2H), 6.71-6.67 (m, 2H),
407 6.33 (d, J = 11.0 Hz, 1H), 6.27-6.24 (m, 1H), 6.19-6.15 (m, 1H), 5.96-5.91 (m, 1H), 5.06 (d, J = 10.7 Hz,
408 1H), 4.91-4.87 (m, 1H), 4.34-4.30 (m, 1H), 4.12-4.09 (m, 1H), 4.03 (q, J = 7.1 Hz, 1H), 3.90 (d, J = 9.3 Hz,
409 1H), 3.73-3.67 (m, 1H), 3.09 (d, J = 10.3 Hz, 1H), 2.93 (m, 1H), 2.87 (s, 3H), 2.82-2.79 (m, 1H), 2.24-2.19
410 (m, 1H), 1.97 (s, 3H), 1.91 (s, 3H), 1.65 (m, 1H), 1.27-1.23 (m, 1H), 0.92-0.90 (m, 1H), 0.86 (dd, J = 10.0,
411 6.9 Hz, 3H), 0.81 (d, J = 6.9 Hz, 3H), 0.47 (d, J = 6.2 Hz, 3H), -0.33 (d, J = 6.9 Hz, 3H); ¹³C-NMR (151
412 MHz, DMSO-*d*₆) δ_C 186.6, 186.0, 172.0, 170.2, 169.5, 148.9, 144.9, 142.9, 139.0, 137.4, 136.5, 135.5,
413 131.7, 131.1, 130.1, 129.0, 125.9, 117.6, 117.4, 115.9, 115.1, 114.0, 108.7, 100.9, 99.5, 76.8, 74.9, 73.4,
414 72.9, 56.6, 47.8, 41.9, 41.2, 40.6, 38.4, 37.5, 36.5, 32.3, 22.6, 20.4, 19.2, 17.8, 11.5, 9.1, 8.9, 8.0; HRMS:
415 found 846.3939, calculated for C₄₆H₅₈N₂O₁₃ 846.3936.

416 **14.** A purple-red solid (61 mg, 71%) *R*_f = 0.25 (EtOAc - MeOH 100:1 v/v); MS *m/z* 870.5 (M⁺1); ¹H-NMR
417 (600 MHz, DMSO-*d*₆) δ_H 10.93 (s, 1H), 8.55 (bs, 1H), 7.53 (q, J = 3.9 Hz, 1H), 7.35 (dd, J = 8.1, 2.9 Hz,
418 1H), 7.24-7.19 (m, 1H), 7.10-7.07 (m, 1H), 7.02-6.96 (m, 1H), 6.34 (d, J = 10.3 Hz, 1H), 6.27-6.24 (m,
419 1H), 6.10-6.05 (m, 1H), 5.93-5.89 (m, 1H), 5.05-4.99 (m, 1H), 4.92 (d, J = 12.1 Hz, 1H), 4.39 (d, J = 12.0
420 Hz, 1H), 4.16 (d, J = 11.0 Hz, 1H), 3.92 (d, J = 8.6 Hz, 1H), 3.75 (d, J = 12.1 Hz, 1H), 3.69 (d, J = 9.0 Hz,
421 1H), 3.24 (d, J = 7.9 Hz, 1H), 3.10-3.05 (m, 1H), 2.91 (s, 3H), 2.83-2.80 (m, 1H), 2.29-2.24 (m, 1H), 1.99

422 (s, 3H), 1.92 (s, 3H), 1.91 (s, 3H), 1.65 (s, 3H), 1.25-1.23 (m, 1H), 1.01-0.98 (m, 1H), 0.91 (d, J = 7.2 Hz,
423 1H), 0.81 (d, J = 6.9 Hz, 3H), 0.30 (d, J = 6.9 Hz, 3H), -0.32 (d, J = 6.9 Hz, 3H); ¹³C-NMR (151 MHz,
424 DMSO-*d*₆) δ_C 185.3, 184.9, 172.0, 170.3, 169.4, 149.2, 148.9, 144.4, 142.4, 137.8, 136.3, 132.1, 131.6,
425 131.4, 131.3, 126.7, 126.1, 123.2, 121.2, 118.5, 118.1, 115.2, 114.6, 111.5, 108.2, 101.3, 97.9, 76.1, 75.7,
426 73.2, 72.8, 55.7, 47.3, 43.0, 40.7, 40.0, 38.1, 37.8, 37.0, 32.6, 29.5, 22.0, 20.0, 19.8, 18.2, 11.1, 9.0, 8.4,
427 7.4; HRMS: found 869.4091 calculated for C₄₈H₅₉N₃O₁₂ 869.4099.

428 **15.** A red solid (65 mg, 73%) *R*_f = 0.23 (EtOAc - MeOH 100:1 v/v); MS *m/z* 895.4 (M⁺1); ¹H-NMR (600
429 MHz, DMSO-*d*₆) δ_H .24 (s, 1H), 8.74 (s, 1H), 8.56 (s, 1H), 8.00 (d, J = 8.6 Hz, 2H), 7.71 (d, J = 8.6 Hz,
430 2H), 6.28 (d, J = 14.5 Hz, 1H), 6.19-6.13 (m, 1H), 5.93 (dd, J = 16.2, 5.9 Hz, 1H), 5.07 (dd, J = 10.8, 4.6
431 Hz, 1H), 5.03-5.01 (m, 1H), 4.97 (dd, J = 11.0, 4.1 Hz, 1H), 4.90-4.86 (m, 1H), 4.17 (s, 1H), 4.05-4.02 (m,
432 2H), 3.90 (d, J = 10.0 Hz, 1H), 3.73 (d, J = 6.5 Hz, 1H), 3.59-3.55 (m, 1H), 3.23 (d, J = 5.5 Hz, 1H), 3.21
433 (s, 3H), 2.87 (s, 3H), 2.80 (d, J = 5.2 Hz, 1H), 2.25-2.18 (m, 1H), 1.99 (s, 3H), 1.94 (d, J = 2.8 Hz, 3H),
434 1.91 (s, 3H), 1.65 (d, J = 5.9 Hz, 3H), 1.63-1.61 (m, 1H), 1.23 (s, 1H), 0.96 (d, J = 3.8 Hz, 1H), 0.90 (d, J
435 = 7.2 Hz, 3H), 0.80 (dd, J = 6.7, 1.9 Hz, 3H), 0.45 (d, J = 6.9 Hz, 3H), -0.36 (d, J = 6.9 Hz, 3H). ¹³C-NMR
436 (151 MHz, DMSO-*d*₆) δ_C 185.0, 184.6, 172.0, 171.1, 168.5, 167.4, 148.9, 147.0, 146.7, 143.8, 140.4, 138.4,
437 137.4, 133.1, 132.7, 129.7, 129.6, 127.2, 126.0, 117.6, 117.1, 115.8, 114.9, 107.0, 101.1, 77.8, 76.1, 73.7,
438 72.8, 59.7, 56.8, 47.1, 43.4, 41.7, 40.0, 38.3, 33.1, 22.0, 20.6, 19.9, 18.1, 10.9, 8.8, 8.3, 7.4; HRMS: found
439 894.3602 calculated for C₄₆H₅₈N₂O₁₄S 894.3609.

440 **16.** A dark orange solid (71 mg, 83%) *R*_f = 0.32 (EtOAc - MeOH 100:1 v/v); MS *m/z* 856.0 (M⁺1); ¹H-
441 NMR (600 MHz, DMSO-*d*₆) δ_H 15.60 (s, 1H), 12.51 (s, 1H), 9.49 (s, 1H), 8.80 (s, 1H), 7.11 (m, 1H), 6.24
442 (d, J = 10.7 Hz, 1H), 6.20 (d, J = 12.8 Hz, 1H), 5.90 (dd, J = 15.9, 6.7 Hz, 1H), 5.35 (bs, 1H), 5.06 (d, J =
443 10.7 Hz, 1H), 5.03 (s, 1H), 4.92 (dd, J = 12.7, 8.1 Hz, 1H), 4.18 (d, J = 8.8 Hz, 1H), 3.74-3.72 (m, 1H),
444 3.23 (d, J = 9.1 Hz, 1H), 2.89 (s, 3H), 2.82 (s, 1H), 2.20-2.16 (m, 1H), 1.96 (s, 3H), 1.90 (s, 3H), 1.63 (s,
445 3H), 1.58 (d, J = 7.2 Hz, 1H), 1.34-1.30 (m, 1H), 1.05-1.00 (m, 1H), 0.88 (d, J = 6.8 Hz, 3H), 0.83 (d, J =
446 6.8 Hz, 3H), 0.43 (d, J = 6.8 Hz, 3H), -0.25 (d, J = 6.8 Hz, 3H). HRMS: found 854.4318 calculated for
447 C₄₄H₆₂N₄O₁₃ 854.4313.

448

449 **Microbiology**

450 **Strains and culture**

451 *M. tuberculosis* strains were cultured in Middlebrook 7H9 medium plus OADC (oleic acid, albumen,
452 dextrose, catalase) supplement and 0.05 % w/v Tween 80 (7H9-OADC-Tw). Rifampicin resistant strains
453 from three different backgrounds were used. RIF-R2 (RpoB_{S531L}) was obtained from ATCC (ATCC 35838).

454 RIF-R1 (RpoB_{S522L}) was isolated as a spontaneous rifampicin resistant mutant from H37Rv-LP (ATCC
455 25618) (1, 2). HN-0258218-RM1 (RpoB_{H455D}) was isolated as a spontaneous rifampicin resistant mutant
456 from HN-878.³² Strain HN878 (NR-13647) was obtained through BEI Resources, NIAID, NIH. The *rpoB*
457 gene was sequenced in the resistant isolates to identify mutations.

458

459

460

461 **Determination of minimum inhibitory concentrations**

462 MICs were determined as previously described using OD₅₉₀ as measurement of growth.^{37,38} Briefly,
463 compounds were tested as 10-point 2-fold serial dilutions. Bacterial growth was measured after 5 days in
464 7H9-OADC-Tw. Growth curves were generated using the Levenberg-Marquardt algorithm. MIC₉₀ was
465 defined as the concentration required to inhibit growth by 90% as compared to controls.

466

467 **Molecular modelling**

468 The molecular modelling work was performed using Desmond³⁹ with Maestro⁴⁰ as graphical user interface
469 (GUI) ver 2020-1, AutoDock Vina ver. 1.1.2⁴¹ with VegaZZ ver. 3.2.1.33^{42,43} as GUI, LeDock,⁴⁴ Avogadro
470 ver 1.2.0⁴⁵ and ChemBioOffice ver. 16.0.1.4. All the analysis and image preparations were conducted using
471 Maestro and Discovery Studio Visualizer ver. 20.1.0.19295.⁴⁶

472 The crystal structure of the wild-type *M. tuberculosis* RNAP in a complex with rifampicin (PDB ID:
473 5UHC)³⁴ was used as a target protein to investigate possible interactions of all ligands with the wild type
474 and mutated protein RpoB_{S522L}. Initially, the three dimensional (3D) structures of all analogues were
475 prepared using ChemBioOffice and saved in a .mol2 format, while the 3D structure of the wildtype RNAP
476 was prepared using Protein Preparation Wizard implemented in Maestro by adding hydrogen atoms and
477 setting protonation states of all ionizable groups for pH 7.

478 The system comprising protein in complex with rifampicin, DNA and RNA was used for further evaluations
479 of the analogues binding in the pocket located on the beta subunit in the wild type and mutated protein. The
480 System Builder Tool was utilized to prepare a cubic periodic solvated system using single point charge
481 (SPC) model of water molecules, with box size 15 Å larger than a molecular system in all directions.
482 Adequate number of Na⁺ and Cl⁻ ions were added to neutralize the system and mimic conditions with 0.05
483 M NaCl concentration. Additionally, following previously reported study structure where it was
484 demonstrated that each subunit is relatively independent and that only β subunit be simulated,³⁵ the β

485 subunit in complex with rifampicin was extracted. The truncated system was prepared in the same way as
486 the full system described as above.

487 Initially, the default Desmond “Molecular Dynamics” protocol and OPLS2005 all atoms force field for that
488 include minimization, equilibration and production run steps was used to conduct simulations for 10 ns.
489 Temperature was kept constant at 300 K with the Nose-Hoover thermostats and pressure was maintained
490 with the Martyna–Tobias–Klein barostats within the NPT ensemble.⁴⁷ The cut off value of 9.0 Å was set in
491 calculations of van der Waals and short-range coulombic interactions. The equation of motion was solved
492 with the RESPA integrator, with an inner time step of 2.0 fs and an outer time step of 6.0 fs.⁴⁸ The results
493 were saved as trajectory by storing coordinates and the energies to disk at every 5 ps. The 10 ns MD
494 simulation was carried out to relax the protein and use the final frame of the trajectory as the target structure
495 of the wild type protein for further docking.

496 In the truncated systems, the large conformational change was observed for the protein segment of residues
497 between I1041 and E1153 that resulted in formation of undesired intermolecular protein interactions and
498 unrealistic binding pocket. Therefore, positional restraints with a force constant of 50 kcal mol⁻¹ Å⁻² were
499 applied for all atoms that were away more than 10 Å from bound rifampicin. The 10 ns MD simulation was
500 repeated to relax the protein and use the final frame of the trajectory as the target structure of the wild-type
501 protein for further docking.

502 The final frames of the resulting trajectories were also used to generate 3D structures of the full system
503 with a S531L mutation and only β subunit with a S522L mutation. Maestro function “Mutate residue” was
504 used to change the serine residues (residue numbers 447 and 456 in the 5UHC entry) into leucine. The
505 modified protein systems were subjected to the protocol for building solvated systems and prepared for the
506 molecular dynamics simulation using the same procedure and settings as for the systems containing wild
507 type structure. Additional 50 ns of the full system and 150 ns of the truncated system production runs NPT
508 simulations were conducted to explore possible effects of mutation on the interactions of residues from the
509 binding site with the rifampicin and analogues. The final frame of the extended simulation trajectories were
510 extracted and used as a target in the molecular docking.

511 The 3D structures of rifampicin analogues were initially built by modifying the previously determined X-
512 ray structure of zwitterionic analog of rifampicin.⁴⁹ These structures were further fully optimized using
513 MOPAC software and PM7 Hamiltonian,⁵⁰ and saved as mol2. The protein structures extracted from crystal
514 structure (PDB ID 5UHC)³⁴ and final frames of the trajectories were used as targets in the docking with the
515 binding sites positioned in the geometrical centers of a bound rifampicin. The docking of ligands in
516 zwitterionic form was conducted using LeDock software. The center of the 20 Å × 20 Å × 20 Å box was
517 positioned on the rifampicin ligand and 20 poses were generated for each analogue. The additional Root

518 Mean Square Deviation (RMSD) cutoff of 1 Å was set to redundancy of poses. The reliability of the docking
519 simulations was demonstrated by redocking rifampicin into the binding site and reproducing the binding
520 modes of the ligand crystal structure within RMSD of 0.7 Å. The largest change of the molecule was
521 observed for piperazine moiety as it is highly dependent on the RNA conformation that changes during the
522 molecular dynamics simulation.

523 **Acknowledgment**

524 Kyle Krieger and Renee Allen are thanked for technical assistance.

525 **Supporting Information**

526 NMR spectral data for **8-16**. Molecular docking scores for neutral rifampicin analogues against *M.*
527 *tuberculosis* H37Rv RpoB and images showing the binding modes of selected analogues within the binding
528 pocket of the β-subunit of wild-type *M. tuberculosis* RNAP.

529 **References**

- 530 1. Sensi, P.; Margalith, P.; Timbal, M. T. Rifomycin, a new antibiotic; preliminary report.
531 *Farmaco. [Sci.]* **1959**, *14*, 146.
- 532 2. McHugh, T. D. *Tuberculosis: Diagnosis and Treatment*; Cabi: 2013; Vol. 21.
- 533 3. Lester, W. Rifampin: A Semisynthetic Derivative of Rifamycin-A Prototype for the Future.
534 *Annu. Rev. Microbiol.* **1972**, *26*, 85-102.
- 535 4. Sensi, P. History of the development of rifampin. *Rev. Infect. Dis.* **1983**, *5*, S402-S406.
- 536 5. Maggi, N.; Pasqualucci, C. R.; Ballotta, R.; Sensi, P. Rifampicin: a new orally active
537 rifamycin. *Chemotherapy* **1966**, *11*, 285-292.
- 538 6. Arioli, V.; Berti, M.; Carniti, G.; Randisi, E.; Rossi, E.; Scotti, R. Antibacterial activity of DL
539 473, a new semisynthetic rifamycin derivative. *J. Antibiot.* **1981**, *34*, 1026-1032.
- 540 7. O'Brien, R. J.; Lyle, M. A.; Snider Jr, D. E. Rifabutin (ansamycin LM 427): a new rifamycin-S
541 derivative for the treatment of mycobacterial diseases. *Rev. Infect. Dis.* **1987**, *9*, 519-530.
- 542 8. World Health Organization No title. *World Health Organization model list of essential*
543 *medicines: 21st list 2019* **2019**.
- 544 9. Lounis, N.; Roscigno, G. In vitro and in vivo activities of new rifamycin derivatives against
545 mycobacterial infections. *Curr. Pharm. Des.* **2004**, *10*, 3229-3238.
- 546 10. Aristoff, P. A.; Garcia, G. A.; Kirchhoff, P. D.; Showalter, H. H. Rifamycins—obstacles and
547 opportunities. *Tuberculosis* **2010**, *90*, 94-118.

- 548 11. Vischer, W. A.; Imhof, P.; Hauffe, S.; Degen, P. Pharmacokinetics of new long-acting
549 rifamycin-derivatives in man. *Bull. Int. Union Tuberc.* **1986**, *61*, 8.
- 550 12. Ramaswamy, S.; Musser, J. M. Molecular genetic basis of antimicrobial agent resistance
551 in *Mycobacterium tuberculosis*: 1998 update. *Tubercle Lung Dis.* **1998**, *79*, 3-29.
- 552 13. Unissa, A. N.; Hanna, L. E. Molecular mechanisms of action, resistance, detection to the
553 first-line anti tuberculosis drugs: Rifampicin and pyrazinamide in the post whole genome
554 sequencing era. *Tuberculosis* **2017**, *105*, 96-107.
- 555 14. World Health Organization. *Global tuberculosis report 2019. Geneva (Switzerland): World
556 Health Organization; 2020* **2020**.
- 557 15. Campbell, E. A.; Korzheva, N.; Mustaev, A.; Murakami, K.; Nair, S.; Goldfarb, A.; Darst, S.
558 A. Structural mechanism for rifampicin inhibition of bacterial RNA polymerase. *Cell* **2001**,
559 *104*, 901-912.
- 560 16. Feklistov, A.; Mekler, V.; Jiang, Q.; Westblade, L. F.; Irschik, H.; Jansen, R.; Mustaev, A.;
561 Darst, S. A.; Ebright, R. H. Rifamycins do not function by allosteric modulation of binding
562 of Mg²⁺ to the RNA polymerase active center. *Proc. Natl. Acad. Sci. U. S. A.* **2008**, *105*,
563 14820-14825.
- 564 17. Berrada, Z. L.; Lin, S. G.; Rodwell, T. C.; Nguyen, D.; Schecter, G. F.; Pham, L.; Janda, J.
565 M.; Elmaraachli, W.; Catanzaro, A.; Desmond, E. Rifabutin and rifampin resistance levels
566 and associated *rpoB* mutations in clinical isolates of *Mycobacterium tuberculosis* complex.
567 *Diagn. Microbiol. Infect. Dis.* **2016**, *85*, 177-181.
- 568 18. Jamieson, F. B.; Guthrie, J. L.; Neemuchwala, A.; Lastovetska, O.; Melano, R. G.; Mehaffy,
569 C. Profiling of *rpoB* Mutations and MICs for Rifampin and Rifabutin in *Mycobacterium*
570 *tuberculosis*. *J. Clin. Microbiol.* **2014**, *52*, 2157.
- 571 19. Czerwonka, D.; Domagalska, J.; Pyta, K.; Kubicka, M. M.; Pecyna, P.; Gajecka, M.;
572 Przybylski, P. Structure–activity relationship studies of new rifamycins containing l-amino
573 acid esters as inhibitors of bacterial RNA polymerases. *Eur. J. Med. Chem.* **2016**, *116*, 216-
574 221.
- 575 20. Pyta, K.; Janas, A.; Szukowska, M.; Pecyna, P.; Jaworska, M.; Gajecka, M.; Bartl, F.;
576 Przybylski, P. Synthesis, docking and antibacterial studies of more potent amine and
577 hydrazone rifamycin congeners than rifampicin. *Eur. J. Med. Chem.* **2019**, *167*, 96-104.
- 578 21. Pyta, K.; Przybylski, P.; Wicher, B.; Gdaniec, M.; Stefańska, J. Intramolecular proton
579 transfer impact on antibacterial properties of ansamycin antibiotic rifampicin and its new
580 amino analogues. *Org. biomol. chem.* **2012**, *10*, 2385-2388.

- 581 22. Pyta, K.; Przybylski, P.; Klich, K.; Stefańska, J. A new model of binding of rifampicin and
582 its amino analogues as zwitterions to bacterial RNA polymerase. *Org. biomol. chem.* **2012**,
583 *10*, 8283-8297.
- 584 23. Pyta, K.; Klich, K.; Domagalska, J.; Przybylski, P. Structure and evaluation of antibacterial
585 and antitubercular properties of new basic and heterocyclic 3-formylrifamycin SV
586 derivatives obtained via 'click chemistry' approach. *Eur. J. Med. Chem.* **2014**, *84*, 651-676.
- 587 24. Cricchio, R.; Tamborini, G.; Bravo, P.; Gaudiano, G. The reaction of 3-formylrifamycin SV
588 with sulphonium and phosphonium ylides. *Farmaco. [Sci.]* **1974**, *29*, 358-365.
- 589 25. Taguchi, M.; Aikawa, N.; Tsukamoto, G. Reaction of 3-formylrifamycin S with secondary
590 amines. *Chemical and pharmaceutical bulletin* **1984**, *32*, 4388-4395.
- 591 26. Bujnowski, K.; Synoradzki, L.; Zevaco, T. A.; Dinjus, E.; Augustynowicz-Kopeć, E.;
592 Napiorkowska, A. Rifamycin antibiotics—new compounds and synthetic methods. Part 4:
593 Study of the reaction of 3-formylrifamycin SV with secondary amines and ketones.
594 *Tetrahedron* **2015**, *71*, 158-169.
- 595 27. Gill, S. K.; Xu, H.; Kirchhoff, P. D.; Cierpicki, T.; Turbiak, A. J.; Wan, B.; Zhang, N.; Peng,
596 K.; Franzblau, S. G.; Garcia, G. A. Structure-based design of novel benzoxazinorifamycins
597 with potent binding affinity to wild-type and rifampin-resistant mutant *Mycobacterium*
598 tuberculosis RNA polymerases. *J. Med. Chem.* **2012**, *55*, 3814-3826.
- 599 28. Dickinson, J. M.; Mitchison, D. A. In vitro activity of new rifamycins against rifampicin-
600 resistant *M. tuberculosis* and MAIS-complex mycobacteria. *Tubercle* **1987**, *68*, 177-182.
- 601 29. Floss, H. G.; Yu, T. Rifamycin mode of action, resistance, and biosynthesis. *Chem. Rev.*
602 **2005**, *105*, 621-632.
- 603 30. Pyta, K.; Janas, A.; Skrzypczak, N.; Schilf, W.; Wicher, B.; Gdaniec, M.; Bartl, F.;
604 Przybylski, P. Specific Interactions between Rifamycin Antibiotics and Water Influencing
605 Ability To Overcome Natural Cell Barriers and the Range of Antibacterial Potency. *ACS*
606 *infectious diseases* **2019**, *5*, 1754-1763.
- 607 31. Pyta, K.; Przybylski, P.; Bartl, F. Regioselective Long-Range Proton Transfer in New
608 Rifamycin Antibiotics: A Process in which Crown Ethers Act as Stronger Brønsted Bases
609 than Amines. *ChemPhysChem* **2015**, *16*, 938-942.
- 610 32. Ioerger, T. R.; O'Malley, T.; Liao, R.; Guinn, K. M.; Hickey, M. J.; Mohaideen, N.; Murphy,
611 K. C.; Boshoff, H. I.; Mizrahi, V.; Rubin, E. J. Identification of new drug targets and
612 resistance mechanisms in *Mycobacterium tuberculosis*. *PLoS one* **2013**, *8*, e75245.
- 613 33. Manca, C.; Tsenova, L.; Bergtold, A.; Freeman, S.; Tovey, M.; Musser, J. M.; Barry, C. E.;
614 Freedman, V. H.; Kaplan, G. Virulence of a *Mycobacterium tuberculosis* clinical isolate in

- 615 mice is determined by failure to induce Th1 type immunity and is associated with induction
616 of IFN- α/β . *Proc. Natl. Acad. Sci. U. S. A.* **2001**, *98*, 5752-5757.
- 617 34. Lin, W.; Mandal, S.; Degen, D.; Liu, Y.; Ebright, Y. W.; Li, S.; Feng, Y.; Zhang, Y.;
618 Mandal, S.; Jiang, Y. Structural basis of Mycobacterium tuberculosis transcription and
619 transcription inhibition. *Mol. Cell* **2017**, *66*, 169-179. e8.
- 620 35. Zhang, Q.; Tan, S.; Xiao, T.; Liu, H.; Shah, S. J. A.; Liu, H. Probing the molecular
621 mechanism of rifampin resistance caused by the point mutations S456L and D441V on
622 Mycobacterium tuberculosis RNA polymerase through Gaussian accelerated molecular
623 dynamics simulation. *Antimicrob. Agents Chemother.* **2020**, *64*.
- 624 36. Artsimovitch, I.; Vassylyeva, M. N.; Svetlov, D.; Svetlov, V.; Perederina, A.; Igarashi, N.;
625 Matsugaki, N.; Wakatsuki, S.; Tahirov, T. H.; Vassylyev, D. G. Allosteric modulation of the
626 RNA polymerase catalytic reaction is an essential component of transcription control by
627 rifamycins. *Cell* **2005**, *122*, 351-363.
- 628 37. Ioerger, T. R.; Feng, Y.; Ganesula, K.; Chen, X.; Dobos, K. M.; Fortune, S.; Jacobs, Jr. W.
629 R.; Mizrahi, V.; Parish, T.; Rubin, E.; Sasseti, C.; Sacchetti, J. C. Variation among
630 genome sequences of H37Rv strains of *Mycobacterium tuberculosis* from multiple
631 laboratories. *J. Bacteriol* **2010**, *192*(14), 3645-3653.
- 632 38. Ollinger, J.; Bailey, M. A.; Moraski, G. C.; Casey, A.; Florio, S.; Alling, T.; Miller, M. J.;
633 Parish, T. A Dual read-out assay to evaluate the potency of compounds active against
634 *Mycobacterium tuberculosis*. *PLoS One* **2013**, *8*, e60531.
- 635 39. Bowers, K. J.; Chow, D. E.; Xu, H.; Dror, R. O.; Eastwood, M. P.; Gregersen, B. A.;
636 Klepeis, J. L.; Kolossvary, I.; Moraes, M. A.; Sacerdoti, F. D. In *In Scalable algorithms for*
637 *molecular dynamics simulations on commodity clusters*; SC'06: Proceedings of the 2006
638 ACM/IEEE Conference on Supercomputing; IEEE: 2006; pp 43.
- 639 40. Schrödinger Release 2020-1: Desmond Molecular Dynamics System, D. E. Shaw Research,
640 New York, NY, 2020. Maestro-Desmond Interoperability Tools, Schrödinger, New York,
641 NY, 2020.
- 642 41. Trott, O.; Olson, A. J. AutoDock Vina: improving the speed and accuracy of docking with a
643 new scoring function, efficient optimization, and multithreading. *Journal of computational*
644 *chemistry* **2010**, *31*, 455-461.
- 645 42. Pedretti, A.; Villa, L.; Vistoli, G. VEGA—an open platform to develop chemo-bio-
646 informatics applications, using plug-in architecture and script programming. *J. Comput.*
647 *Aided Mol. Des.* **2004**, *18*, 167-173.
- 648 43. Pedretti, A.; Villa, L.; Vistoli, G. VEGA: a versatile program to convert, handle and
649 visualize molecular structure on Windows-based PCs. *J. Mol. Graph. Model.* **2002**, *21*, 47-
650 49.

- 651 44. Zhang, N.; Zhao, H. Enriching screening libraries with bioactive fragment space. *Bioorg.*
652 *Med. Chem. Lett.* **2016**, *26*, 3594-3597.
- 653 45. Hanwell, M. D.; Curtis, D. E.; Lonie, D. C.; Vandermeersch, T.; Zurek, E.; Hutchison, G. R.
654 Avogadro: An advanced semantic chemical editor, visualization, and analysis platform *J.*
655 *Cheminformatics* **2012**, *4*, 1-17.
- 656 46. Dassault Systèmes BIOVIA, Discovery Studio Modeling Environment, Release 2017, San
657 Diego: Dassault Systèmes, 2016.
- 658 47. Hoover, W. G. Canonical dynamics: Equilibrium phase-space distributions. *Physical review*
659 *A* **1985**, *31*, 1695.
- 660 48. Humphreys, D. D.; Friesner, R. A.; Berne, B. J. A multiple-time-step molecular dynamics
661 algorithm for macromolecules. *J. Phys. Chem.* **1994**, *98*, 6885-6892.
- 662 49. Wicher, B., Pyta, K., Przybylski, P., Tykarska, E., & Gdaniec, M. Redetermination of
663 rifampicin pentahydrate revealing a zwitterionic form of the antibiotic. *Acta*
664 *Crystallographica Section C*, *68*(5) **2012**, o209-o212. doi:10.1107/S0108270112015296
- 665 50. Stewart J. J. Optimization of parameters for semiempirical methods VI: more modifications
666 to the NDDO approximations and re-optimization of parameters. *Journal of molecular*
667 *modelling* **2013**, *19*(1), 1–32. <https://doi.org/10.1007/s00894-012-1667-x>

668

669

670

671

672

673 **Figure 1.** Structures of rifamycin derivatives developed to treat tuberculosis infections. Rifamycin B (**1**)
674 and SV (**2**) were originally isolated from cultures of *Amycolatopsis rifamycinica* and due to severe side
675 effects were not developed as antibacterial drugs. Rifampicin (**3**, RIF), rifapentine (**4**, RPT) and rifabutin (**5**,
676 RBT) are currently used to treat tuberculosis infected patients. Early rifamycin CGP-7040 (**6**) had longer
677 half-life compared to RIF and showed superior activity against non-tuberculous bacteria (e.g., MAC),
678 although its drug development program was abandoned due to lack of financial incentives. Compound (**7**)
679 is an experimental rifamycin SV derivative bearing a secondary amine unit that showed interesting growth
680 inhibitory properties *in vitro* against *Mtb* H37Rv.

681

682 **Figure 2.** a) ^1H NMR spectrum of **8** within the 5.9-9.5 ppm range recorded in $\text{DMSO-}d_6$ at 600 MHz
683 highlighting the presence of the protonated amino group at C-38. b) ^1H - ^{13}C -HSQC spectrum of **8** in DMSO-
684 d_6 . Spectral region at δ_{H} -0.50 – 7.50.

685

686 **Figure 3a-c.** Binding modes of the new rifamycin analogues within the binding pocket of the whole system
687 of wild type *Mtb* RNAP (3D structure extracted from PDB ID: 5UHC)31 as a target: a) **15** (pink sticks) and
688 **12** (light blue sticks). Amino acid residues of the RNAP binding are shown as thin sticks coloured according
689 to CPK scheme, while the carbon atoms of the nucleotide are coloured in cyan. Key residues that form
690 interactions with the analogues are labelled, while the interactions are shown as dotted lines.

691

692 **Figure 4.** Second favourable binding mode of **15** within the binding pocket of the beta subunit system of
693 wild type *Mtb* RNAP ((3D structure extracted from the molecular dynamics simulation trajectory). Carbon
694 atom of the analogues are coloured in pink and the amino acid residues of the RNAP binding are shown as
695 thin sticks coloured according to CPK scheme. Key residues are labelled, while the interactions are shown
696 as dotted lines.

697

698

699 **Figure 5a-d.** Comparison of the rifampicin binding sites of the *Mtb* RNAP found in the: **a)** crystal structure
700 of the wild type protein (PDB entry 5UHC), **b)** final frame of the trajectory obtained by molecular dynamics
701 simulation of the protein with S531L mutation and **c)** final frame of the trajectory obtained by molecular
702 dynamics simulation of the protein with S522L mutation. Binding sites are shown as spatial distribution of
703 hydrophilicity and hydrophobicity mapped onto a surface. Most of the pocket residues are shown in thin
704 stick representation, with S522, L522, S531 and L531 residues shown as thick sticks and selected
705 hydrophobic residues shown as medium sticks in the mutated protein; **d)** the overlay of the residues of the
706 binding site extracted from the crystal structure³⁴ (green sticks) and S522L structure (grey sticks), where
707 the thickness of the sticks indicates the residues that affected the shape of the binding site in the mutated
708 protein.

709 **Figure 6a -b.** The second favourable docking poses of a) **14** and b) **15** inside the binding site found in the
710 simulated structure of S522L mutated *Mtb* RNAP. The red circle indicates unoccupied spaces of the wild
711 type *Mtb* RNAP as an additional pocket to accommodate the tail of rifampicin analogues. The surface
712 represents the binding site coloured according to its hydrophobicity.

713

714

715

716

717

718

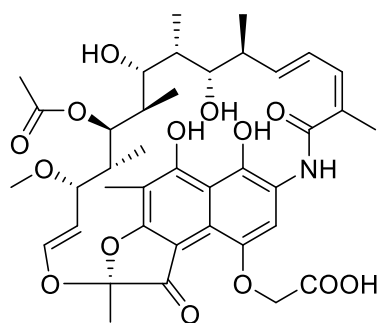
719

720

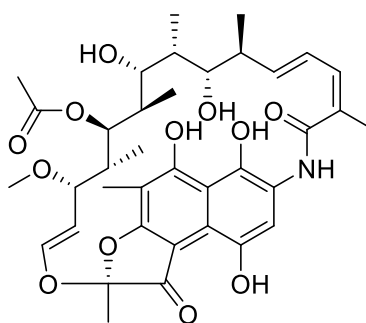
721

722

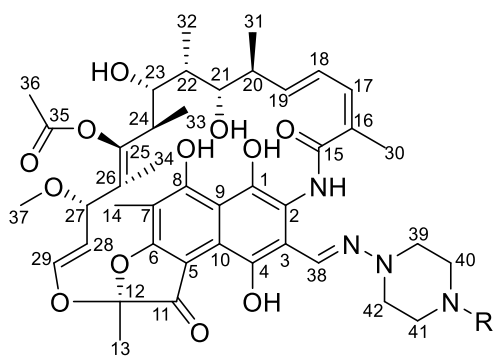
723



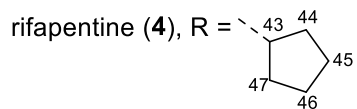
rifamycin B (1)



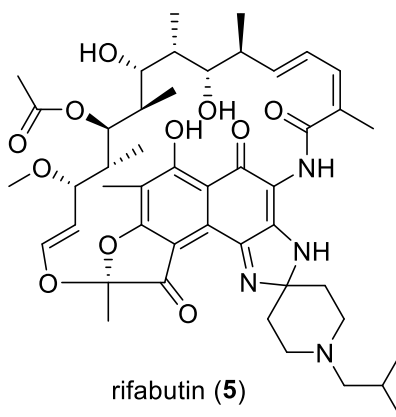
rifamycin SV (2)



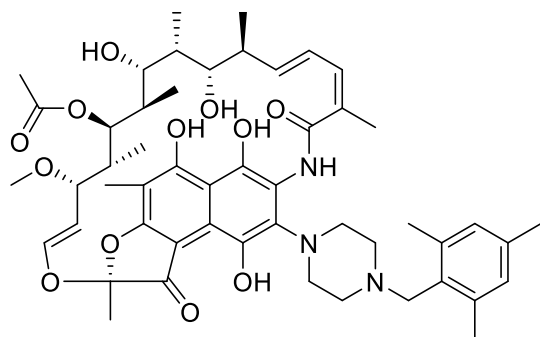
rifampicin (3), R = CH_3



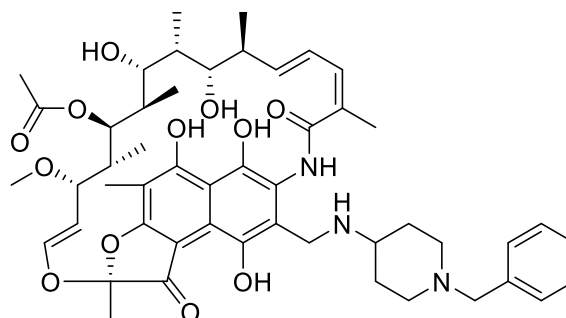
rifapentine (4), R =



rifabutin (5)



CGP-7040 (6)



benzyl-piperidyl rifamycin analogue (7)

725

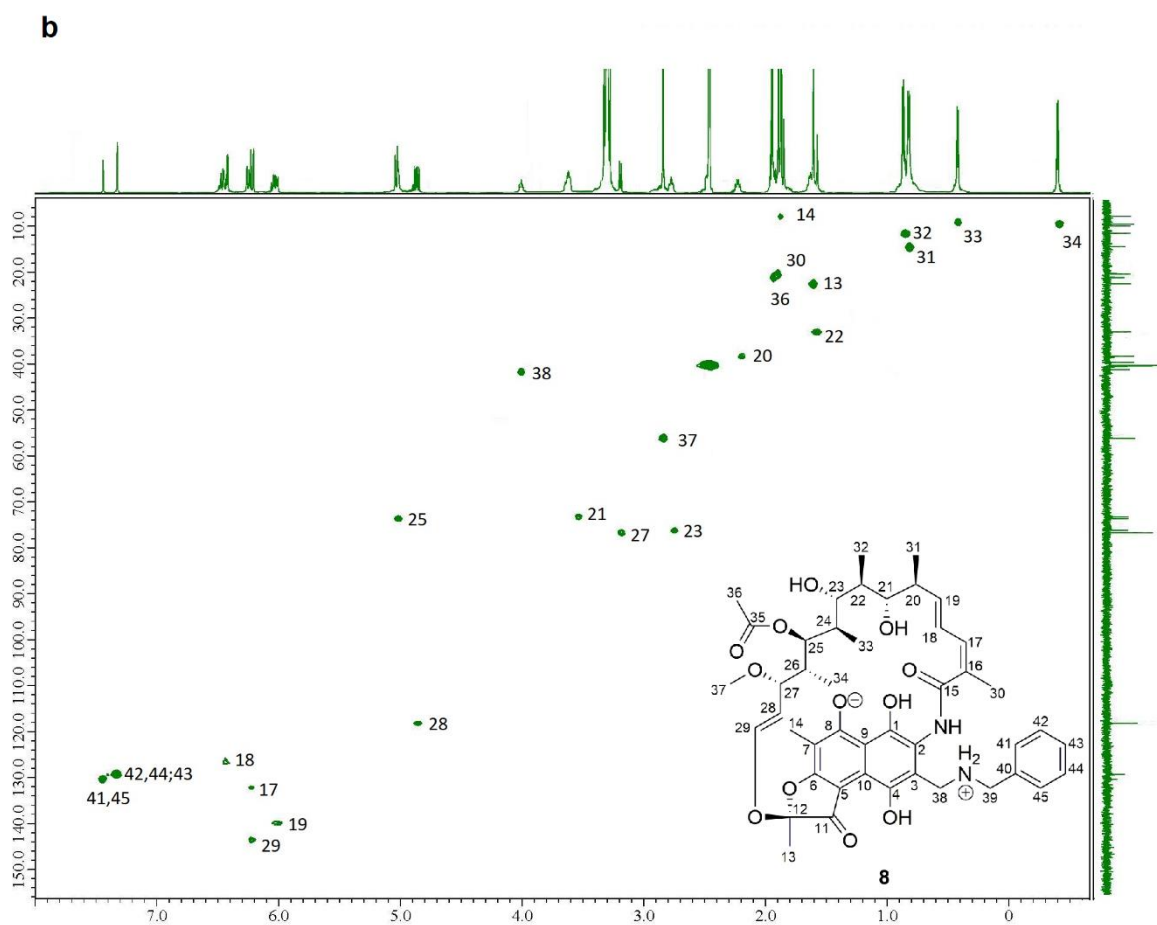
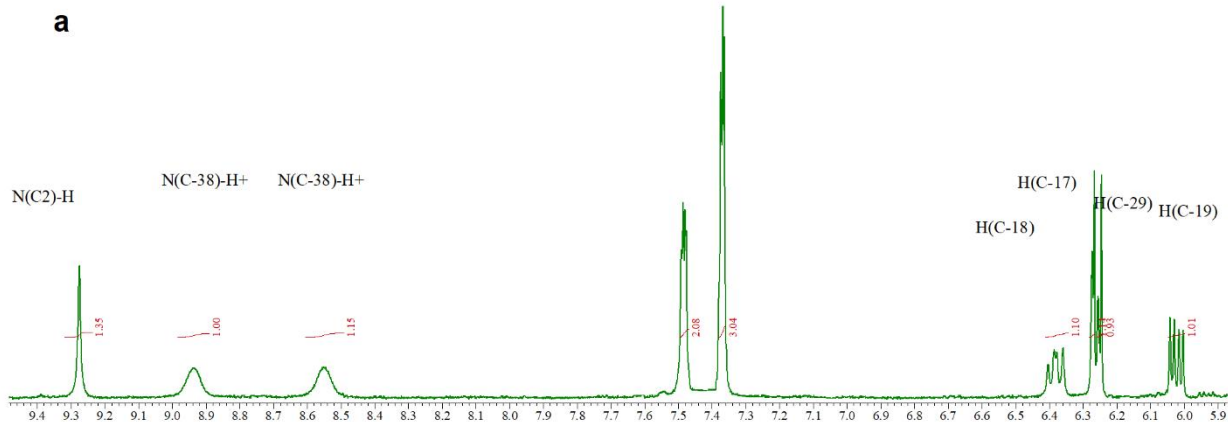
726

727

728

729

730 **Figure 2a-b.**



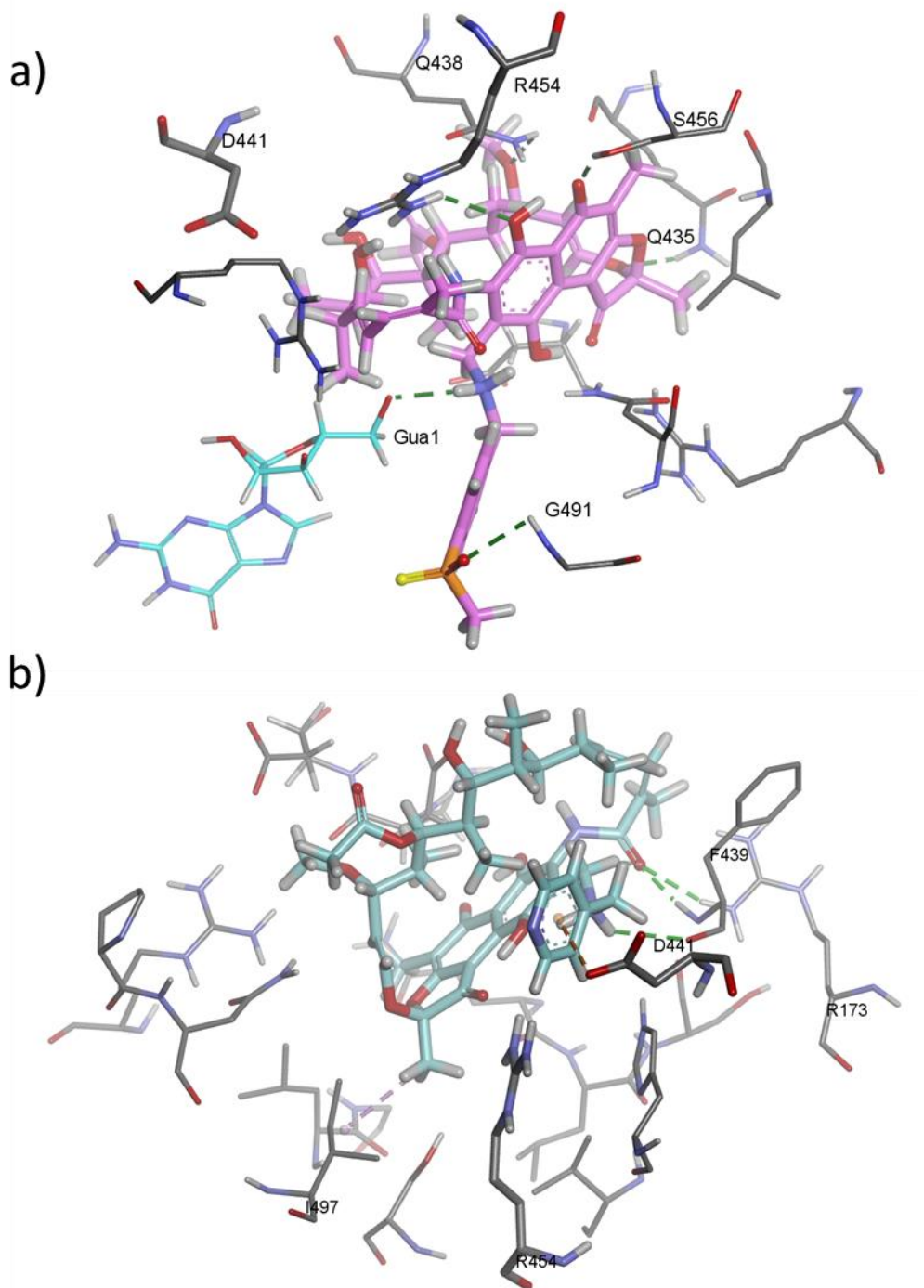
731

732

733

734

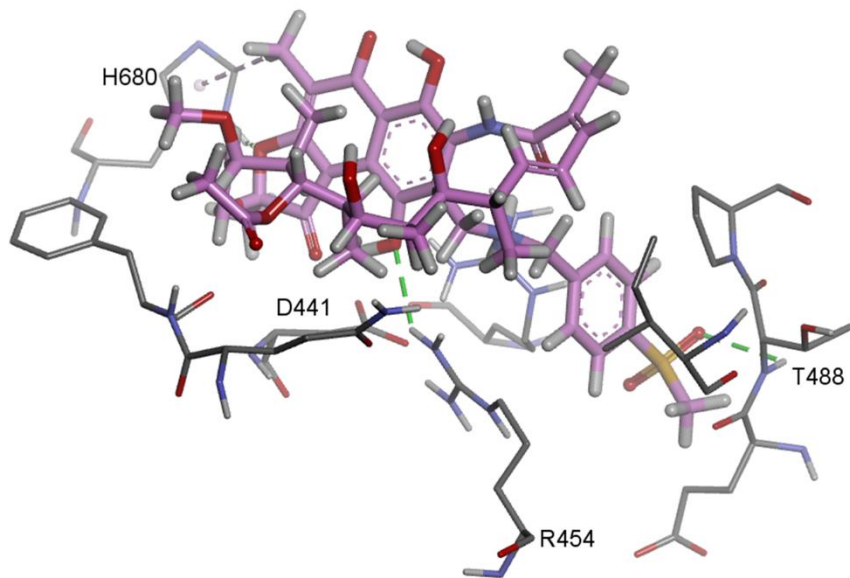
735 **Figure 3.**



736

737

738 **Figure 4.**



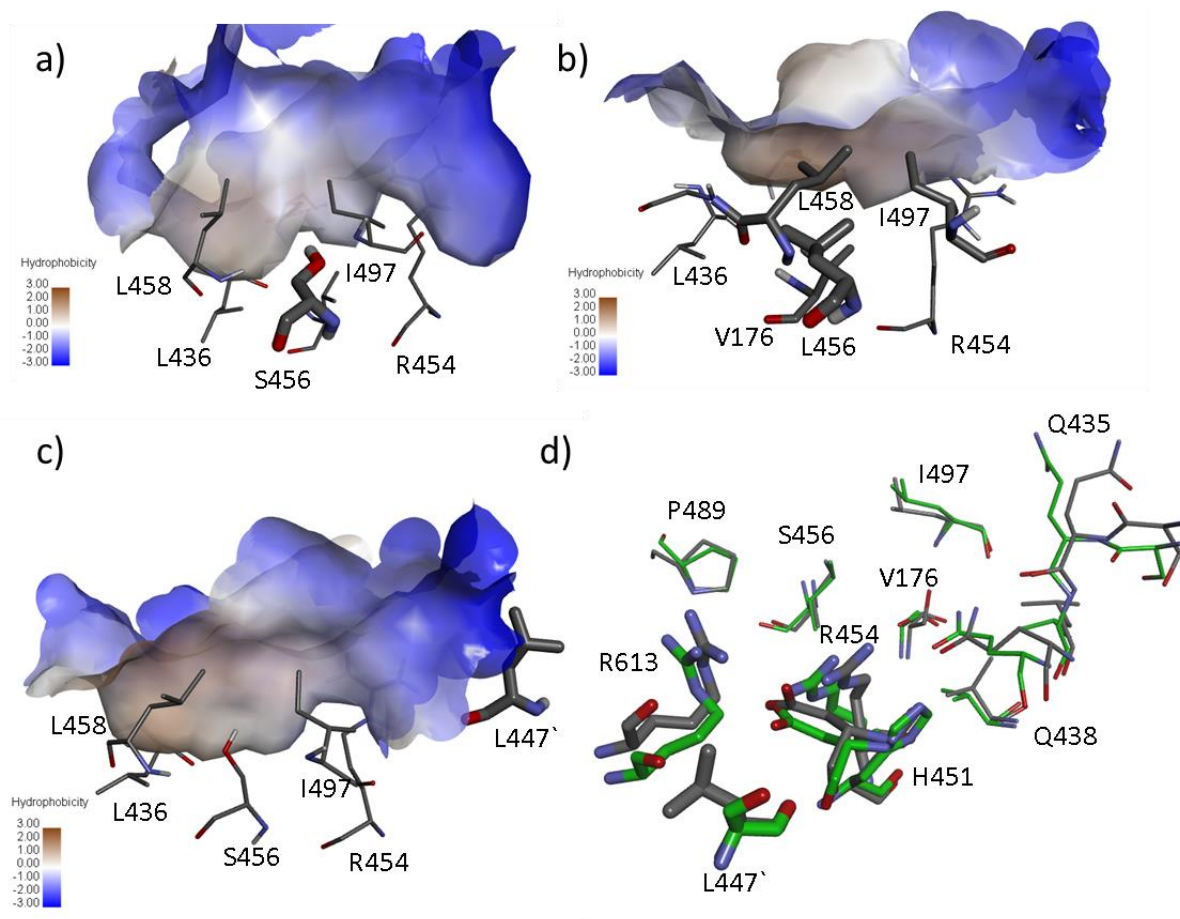
739

740

741

742

743 **Figure 5.**



744

745

746

747

748

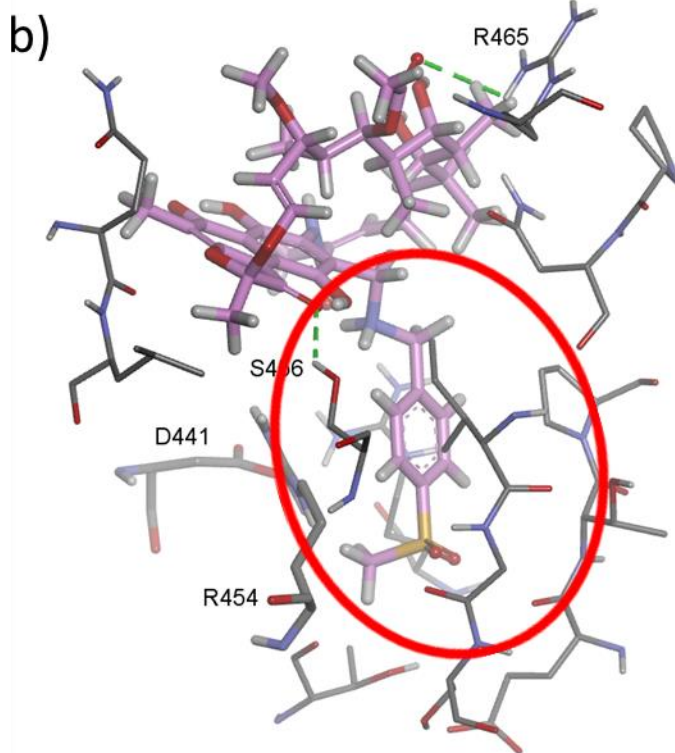
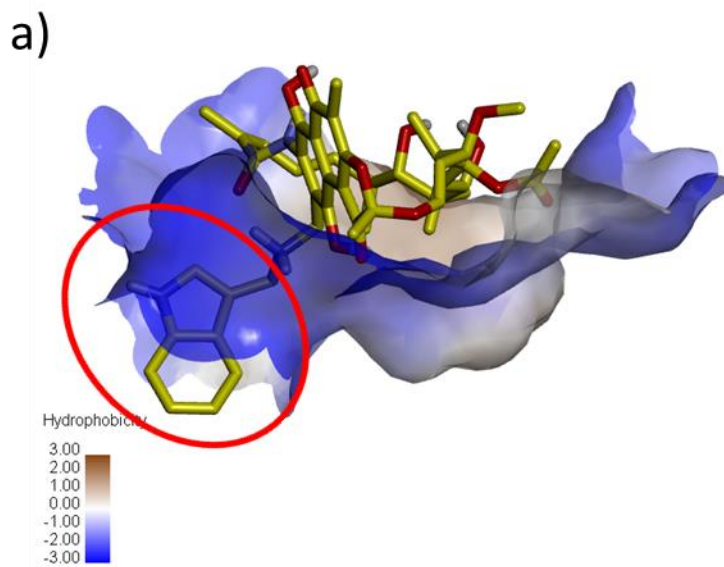
749

750

751

752 **Figure 6.**

753



754

755